Title: A Novel Pan-RAS Inhibitor with a Unique Mechanism of Action Blocks Tumor Growth in Mouse Models of GI Cancer

Authors: [1]Jeremy B. Foote, [2]Tyler E. Mattox, [3,12]Adam B. Keeton,[3,12]Xi Chen, [3]Forrest Smith, [3]Kristy L. Berry, [3]Thomas Holmes, [3]Junwei Wang, [3]Chung-Hui Huang, [2]Antonio B. Ward, Amit K. Mitra[3], [2]Veronica Ramirez-Alcantara, [1]Cherlene Hardy, [4]Karrianne G. Fleten; [4]Kjersti Flatmark; [5]Karina J. Yoon, [6]Sujith Sarvesh, [6]Ganji Purnachandra Nagaraju, [3]Yulia Maxuitenko, [3]Jacob Valiyaveettil, [6]Julienne L. Carstens, [7]Donald J. Buchsbaum, [8]Jennifer Yang, [9]Gang Zhou, [10]Elmar Nurmemmedov, [10]Ivan Babic, [11]Vadim Gaponenko, [11]Hazem Abdelkarim, [12]Michael R. Boyd, [13]Gregory S. Gorman, [14]Upender Manne, [15]Sejong Bae, [6]Bassel F. El-Rayes, and [3,12]Gary A. Piazza

Affiliations: [1]Department of Microbiology, University of Alabama at Birmingham, Birmingham AL, [2]University of South Alabama, Mobile, AL; [3]Department of Drug Discovery and Development, Harrison College of Pharmacy, Auburn University, Auburn, AL;[4] Department of Gastroenterological Surgery, Oslo University Hospital, The Radium Hospital, Oslo, Norway and Institute of Clinical Medicine, Faculty of Medicine, University of Oslo, Oslo, Norway; [5]Department of Pharmacology and Toxicology, University of Alabama at Birmingham, Birmingham AL; [6]Department of Hematology and Oncology, University of Alabama at Birmingham, Birmingham, AL; [7]Department of Obstetrics and Gynecology, University of Alabama at Birmingham, Birmingham, AL; [8]University of Connecticut, Mansfield, CT; [9]Georgia Cancer Center, University of Augusta, Augusta, GA; [10]Celaris Bio LLC, San Diego, CA; [11]Department of Biochemistry and Molecular Genetics, University of Illinois, Chicago, IL; [12]ADT Pharmaceuticals LLC, Orange Beach, AL. [13]Department of Pharmaceutical, Social and Administrative Sciences, McWhorter School of Pharmacy, Samford University; Birmingham, AL, [14]Department of Pathology, University of Alabama at Birmingham, Birmingham, AL; [15]Division of Preventive Medicine, University of Alabama at Birmingham, Birmingham, AL.

Running Title: *A novel pan-RAS inhibitor for RAS-driven GI cancers*

Key Words: KRAS, pan-RAS inhibitor, pancreatic cancer, colorectal cancer, tumor immune microenvironment

Funding Sources: NIH/NCI R01CA254197, R01CA238514, P30CA01314, and Norwegian Cancer Society 197837.

Corresponding Author: Gary A. Piazza, Ph.D. W.W. Walker Endowed Professor, Department Head, Drug Discovery and Development; Director, Cancer Research Center, Harrison College of Pharmacy, Auburn University, Auburn, AL, Walker Building, 362 W. Thach Ave, Room 3306F, 334-844-7409, gap0034@auburn.edu

Disclosure of Potential Conflicts of Interest: G.A. Piazza, A.B. Keeton, X. Chen, and M.R. Boyd are co-founders of ADT Pharmaceuticals Inc. and consultants. All other authors declare no potential conflicts of interest.

ABSTRACT

Here, we describe a novel pan-RAS inhibitor, ADT-007, that potently inhibited the growth of RAS mutant cancer cells irrespective of the RAS mutation or isozyme. RAS^{WT} cancer cells with activated RAS from upstream mutations were equally sensitive. Conversely, cells from normal tissues or RAS^{WT} cancer cells harboring downstream BRAF mutations were insensitive. Insensitivity to ADT-007 was attributed to low activated RAS levels and metabolic deactivation by UDP-glucuronosyltransferases expressed in normal cells but repressed in RAS mutant cancer cells. Cellular, biochemical, and biophysical experiments show ADT-007 binds nucleotide-free RAS to block GTP activation of RAS and MAPK/AKT signaling. Local administration of ADT-007 strongly inhibited tumor growth in syngeneic immune-competent and xenogeneic immune-deficient mouse models of colorectal and pancreatic cancer while activating innate and adaptive immunity in the tumor immune microenvironment. Oral administration of ADT-007 prodrug inhibited tumor growth, supporting further development of this novel class of pan-RAS inhibitors for treating RAS-driven cancers.

SIGNIFICANCE

ADT-007 is a 1st-in-class pan-RAS inhibitor with ultra-high potency and unique selectivity for cancer cells with mutant or activated RAS capable of circumventing resistance and activating antitumor immunity. Further development of ADT-007 analogs or prodrugs with oral bioavailability as a generalizable monotherapy or combined with immunotherapy is warranted.

INTRODUCTION

Colorectal cancer (CRC) and pancreatic ductal adenocarcinoma (PDA) are projected to cause 53,010 and 51,750 deaths in the US in 2024, respectively [1]. The 5-year survival rates for CRC and PDA are 63% and 13%, respectively [1]. Over 50% of CRC and 90% of PDA

patients harbor gain-in-function mutations in KRAS genes that are associated with poor prognosis, making the development of novel RAS inhibitors an urgent unmet medical need [2].

For many cancers, RAS mutations initiate tumorigenesis that in cooperation with the acquisition of mutations in other oncogenes or inactivating mutations in tumor suppressor genes such as p53 [3], SMAD4 [4], APC [5], or p16 [6], drive the progression from precancerous lesions to malignant disease. Signaling through mutant or non-mutant wild-type RAS (RAS^{WT}) is critical for transformation [7], cancer cell proliferation and survival [7, 8], chemoresistance [9], and metastasis [5, 10]. RAS mutations also promote immunosuppression within the tumor immune microenvironment (TiME) through a broad array of mechanisms, including increased production of acute inflammatory cytokines (IL-6, IL-8) [11], priming of immunosuppressive T-regs [12], MDSCs [13], downregulation of MHCI [14], increased expression of programmed cell death ligand 1 (PD-L1) [15], and suppression of intra-tumoral interferon (IFN) signaling [16]. Cumulatively, oncogenic RAS-mediated reprograming of the TiME results in weakened recognition and reduced cytotoxic T and NK cell functions that support tumor progression.

The recent development of drugs directed against cancers harboring KRAS mutations at the G12C and G12D codons has set the stage for selective targeting of KRAS-driven malignancies [17]. Clinical trials evaluating sotorasib (AMG-510) and adagrasib (MRTX-849) selective for the $KRAS^{G12C}$ mutation show promising efficacy for NSCLC patients with mutant $KRAS^{G12C}$ but a lower response rate in patients with $KRAS^{G12C}$ mutant CRC [18]. Preclinical data shows much promise of $KRAS^{G12C}$ and newly developed $KRAS^{G12D}$ inhibitors to rewire the immunosuppressive machinery that limits T cell recognition and cytotoxic activity [19]. However, clinical trials indicate that combining such drugs with checkpoint immunotherapy may not be well tolerated [20]. Adaptive resistance is another limitation of mutant-specific KRAS inhibitors [21]. Resistance may result from new activating mutations involving RAS isozymes (KRAS, HRAS, and NRAS) or activation of RAS^{WT} isozymes from upstream receptor tyrosine kinases (RTK) [22],

making pan-RAS inhibitors an attractive therapeutic option to dampen the RAS-related adaptive resistance circuitry. In addition, the presence of different RAS mutations in the same tumor and the role of RAS^{WT} proteins in oncogenesis [7] expands the potential efficacy advantages of RAS inhibitors capable of inhibiting both mutant RAS and RAS^{WT} activated from upstream signaling molecules.

Here, we characterize a novel pan-RAS inhibitor, ADT-007, with the potential to circumvent resistance and activate antitumor immunity. ADT-007 was discovered from screening a library of compounds that share the indene scaffold of the nonsteroidal anti-inflammatory drug (NSAID), sulindac, previously reported to preferentially inhibit the formation of RAS mutant tumors in a rat model of chemical-induced mammary tumorigenesis [23]. Subsequent studies reported that sulindac binds RAS and inhibits RAS-induced transformation and signaling, albeit with modest potency and confounding inhibition of cyclooxygenase (COX) [24, 25]. The current studies determined the mechanism of action of ADT-007 that lacks COX inhibitory activity yet is ~10,000 fold more potent than sulindac to inhibit cancer cell growth *in vitro*. We also assessed the anticancer activity of ADT-007 using cancer cell lines representative of the complex mutational landscape of RAS-driven cancers and immune modulatory potential using mouse tumor models with different immune compositions representative of the diversity seen in patients with CRC and PDA.

Material and Methods:

<u>Chemical synthesis:</u> ADT-007, (*Z*)-2-(5-fluoro-1-(4-hydroxy-3,5-dimethoxybenzylidene)-2-methyl-1H-inden-3-yl)-N-(furan-2-ylmethyl)acetamide, and ADT-316, (*Z*)-4-((5-fluoro-3-(2-((furan-2-ylmethyl)amino)-2-oxoethyl)-2-methyl-1H-inden-1-ylidene)methyl)-2,6-dimethoxyphenyl 4-methylpiperazine-1-carboxylate hydrochloride, were synthesized as follows: To a 250-mL round-bottom flask equipped with a gas outlet, (Z)-2-(1-(4-acetoxy-3,5-dimethoxybenzylidene)-5-fluoro-2-methyl-1H-inden-3-yl) acetic acid (10.3 g, 25.00 mMol) was

added to 180 mL of anhydrous dichloromethane, followed by carbonyl diimidazole (CDI) (4.25 g, 26.25 mMol). The mixture was stirred for 30 minutes, followed by the addition of furfuryl amine (2.68g, 26.25 mMol) and anhydrous pyridine (20 mL). The solution was stirred at room temperature for 48 hours and washed with 0.2N HCl (120 mL) and water (120 mL x 2). The organic layer was concentrated. The residue was dissolved in 300 mL of methanol, followed by addition of ammonium in methanol (7N, 100 mL). The red mixture was stirred vigorously overnight, then filtrated. The solid was dissolved in 400 mL of ethyl acetate, treated with 1N HCl, and washed with brine (150 mL x 3) and dried over anhydrous sodium sulphate. After filtration the solution was concentrated. The residue was recrystallized from acetone/ethyl acetate to afford the ADT-007 as a yellow crystal. The mother liquor was concentrated. Purification of the residue with silica gel column chromatography, followed by the above recrystallization procedure gave the second crop (9.54 g combined, 85%). Treatment of ADT-007 with 4-methylpiperazine-1-carbonyl chloride in anhydrous pyridine at 50 °C overnight, followed by chromatography purification and acidification afforded ADT-316 HCl as a yellow crystal.

Mice: Eight-week-old female C57BL/6 mice (000664), male and female NOD.Cg-*Prkdc*^{scid} *Il2rg*^{tm1Wjl}/SzJ (NSG, 00557) and female B6.129S7-*Rag1*^{tm1Mom}/J (Rag 1$^{-/-}$, 02216) were purchased from Jackson Laboratory. Female B6.Ifng/Thy1.1 KI (IFN-γ.Thy1.1) and B6.Cg-Tg-IL2$^{tm1(eGFP)/Weav}$ (IL-2.GFP) knock-in cytokine reporter mice were kindly provided by Dr. Casey Weaver (University of Alabama at Birmingham, Birmingham, AL) [39]. 6–8-week-old female athymic foxn1 nude mice were bred at Department of Comparative Medicine, Oslo University Hospital (OUH). Experiments were randomized, but not blinded. All animal experiments and procedures were performed under approved protocols in accordance with guidelines from the University's Institutional Animal Care & Use Committee (IACUC). For animal studies performed at OUH Institute for Cancer Research (Norwegian Radium Hospital, Oslo, Norway) all procedures and experiments involving animals were approved by the Norwegian Food Safety

Authority (application ID #18209) and were conducted according to the recommendations of the European Laboratory Animals Science Association and the ARRIVE guidelines.

Cell lines and patient derived xenografts: Murine PDA cell lines were derived from tumor-bearing $Kras^{LSL\text{-}G12D/+}$; $Trp53^{LSL\text{-}R172H/+}$; Pdx1-Cre; $Rosa26^{YFP/YFP}$ (7160c2, 2838c3) and $Kras^{LSL\text{-}G12D/+}$; $Trp53^{L/+}$; Pdx1-Cre (5363) mice and cultured in DMEM complete media as previously indicated [36]. Human tumor cell lines (BxPC-3, AsPC-1, CFPAC1, MIA PaCa-2, PANC-1, SW-1990, HT-29, HCT-116, A-549, SW-480, MDA-MB-231, OVCAR-8, Hs578T, SK-MEL2, H-1299, OV-90, H-1975, U87-MG, SK-OV3), and the murine tumor lines (B16 melanoma and Lewis lung cancer) were purchased from ATCC and maintained according to ATCC guidelines. The normal lung epithelial cells (NHAEC) were purchased from Lonza and cultured using bronchial epithelial growth medium per the supplier's protocol. NCM-460 cells were obtained from InCell (San Antonio) and maintained in medium/nutrient mixture with 10% FBS for less than 12 passages, according to the supplier's protocol. The human gall bladder adenocarcinoma expressing $KRAS^{G12V}$ was derived from an 80-year-old male patient, with previous history of pancreatic cancer. Originally diagnosed as PDA, the tumor was reclassified as a gall bladder adenocarcinoma. This PDX model was serially passaged in NSG mice. The CRC PDX models were established by implanting peritoneal metastasis samples collected at the time of cytoreductive surgery – hyperthermic intraperitoneal chemotherapy (CRS-HIPEC) into the peritoneal cavity of nude mice. The PMP-1 model was established from a patient with an appendiceal primary lesion, while PMCA-1 was from a patient with a primary mucinous rectal carcinoma [51, 52]. The PC244 model was established from a peritoneal metastasis specimen from a 69-year-old female with a poorly differentiated mucinous adenocarcinoma of the cecum. Targeted next-generation sequencing of PC244 was performed as previously described [53]

For studies performed at UAB and University of South Alabama (USA), all cell lines and PDX models were tested against an extended panel of excluded pathogens including mycoplasma prior to *in vivo* studies as mandated by UAB and USA IACUC and ARP guidelines.

Tumor cell transfections: BxPC-3 and HT-29 cells were initially exposed to lentiviral particles containing a mutant HRAS^{G12V} or *KRAS*^{G12C} construct for 48 hours in a 6-well plate at 37°C in a humidified incubator with 5% carbon dioxide. The media was then removed and replenished with fresh media containing HA-*HRAS*^{G12V} or HA-*KRAS*^{G12C} lentiviral particles. After another 48 hours, the media was removed, and fresh media containing 5 µg/mL puromycin was added to the well. Surviving cells were expanded in a 10 cm dish, and expression of the construct was confirmed by WB with an HA tag antibody (Cell Signaling Technology).

HEK 293FT (Invitrogen, # R70007) cell line was transfected with either pBabe-puro-HA-KRASG12C (Addgene, #58901) or pBabe-puro-Empty (Addgene, #1764) retroviral constructs along with pCL-10A1 retrovirus packaging vector (Novus Biologicals, # NBP2-29542). Following a 48-h incubation at 37°C, culture supernatants containing viral particles were collected and mixed with PEG-itTM (SBI, #LV810A-1) virus precipitation reagent (5X) followed by overnight incubation at 4°C. Thereafter, supernatants were centrifuged at 1500 x g for 30 min and white pellets of retroviral particles containing either pBabe-puro-HA-KRAS G12C or pBabe-puro-Empty retroviral construct were collected and resuspended in sterile phosphate buffered saline (PBS). BxPC-3 cells were transduced with retroviral particles in a 6-well plate using polybrene transfection reagent (EMD MIllipore, TR-1003-G) and incubated for 48 h at 37°C. Thereafter, media was replaced with fresh media containing 5 µg/mL puromycin. Surviving cells were selected, expanded, and confirmed for KRAS^{G12C} expression by WB using an HA tag antibody (Cell Signaling Technology).

ADT-007 treatment and EGF stimulation: For *in vitro* ADT-007 studies, cell cultures were incubated with increasing concentrations (0.1, 0.5, 1, 5, 10, 50, 100, 250, 500, 1000, 10000 nM)

of ADT-007, AMG-510 (Selleck Chemicals, Houston, TX) or MRTX849 (Selleck Chemicals, Houston, TX) or vehicle (DMSO) for a period of 24 – 72 hours depending on the assay. In some experiments, recombinant mouse EGF (Gibco, Jenks, OK) was added 10 minutes prior to harvesting protein lysates from treated tumor cell lines to assess the impact of upstream receptor tyrosine kinase signaling on RAS-MAPK and RAS-PI3K pathways.

Cell growth assays: To determine 2D growth IC_{50} values, 5 x 10^3 tumor cells were plated in triplicate in 96 well flat bottom plate. To determine 3D growth IC_{50} values, 1 x 10^3 tumor cells were plated in triplicate in 96 well round bottom non-binding plate. Cultures were incubated with various concentrations of ADT-007 (0.1. 0.5. 1, 5, 10, 50, 100, 250, 500, 1000, 10000 nM) and cultured for an appropriate period depending on cellular growth kinetics as indicated in figure legends. At 72-96 hours (2D) or 8-10 days (3D spheroid), cells were processed according to the manufacturer's recommendations to assess intra-cellular ATP levels as a measure of cellular proliferation and viability using CellTiter-Glo (Promega, Madison, WI). Nonlinear dose-response curves showing the effects of compound concentration on colony count were generated using GraphPad Prism.

Gene expression database analysis: Transcriptomic (RNAseq data) for most of the cell lines in Table 1 is publicly available in Cancer Cell Line Encyclopedia accessed via the DepMap Portal) [30]. The Student's T-test was used to identify significant differences in 19,221 TPM+1 normalized transcripts between the two categories of cell lines. Due to the modest number of resistant lines available, a threshold of $p < 0.01$ was chosen, which identified 719 transcripts and was reduced to 254, unique transcripts expressed at least a 5-fold difference.

NMR Spectroscopy: Recombinant WT KRAS was dialyzed 2X for 24 hours (12 hours each in 1L 50 mM Tris-Citrate pH=6.5, 50 mM NaCl, 10 mM β-mercaptoethanol) at 4 ºC following treatment with 10 mM EDTA to remove Mg^{2+} and the bound nucleotide. To record ^{1}H-^{15}N heteronuclear single quantum coherence (HSQC) NMR spectra of nfKRAS we used 900 MHz and 600 MHz

Avance spectrometers (Bruker, Billerica, MA, USA), equipped with cryogenic probes. Each *in vitro* experiment was performed at 25°C in 50 mM Tris-Citrate pH=6.5, 50 mM NaCl, 10 mM β-mercaptoethanol containing 10% $^{2}H_2O$. The chemical shift assignments were taken from the Biological Magnetic Resonance Data Bank (BMRB) database (http://www.bmrb.wisc.edu) by use of the BMRB accession numbers: 18529, 25114, and 26635. Chemical shift perturbations higher than the sum of the average and 1 SD were considered to be statistically significant.

Nucleotide Exchange Assays: The fluorescent GTP analog MANT-GTP was purchased from Millipore Sigma. For each reaction, 5 µL of 5 µM purified GDP-bound K-RAS in reaction buffer (40 mM Tris-HCl, 100 mM NaCl, 20 mM MgCl, 1 mg/mL BSA, pH 7.5) and 2.5 µL of 200 mM EDTA was added to a microcentrifuge tube to make a master mix. Water was used in place of EDTA in some reactions as a control for the release of GDP. 7.5 µL of master mix per well was added to a 384-well plate for each respective reaction. 5 µL of compound at five times the desired concentration or vehicle in reaction buffer was added to each respective well. After 2.5 minutes for equilibration at 26°C in a Bio-Tek Synergy H4 microplate reader, 12.5 µL of 1.5 µM MANT-GTP in reaction buffer was added to each well for a final concentration of 750 nM MANT-GTP, 1 µM RAS, 20 mM EDTA, and the desired concentration of compound or vehicle. In the case of compound preincubation, the plate was incubated for 1 hour at 26°C prior to MANT-GTP addition. Fluorescence was measured at an excitation wavelength of 360 nm and an emission wavelength of 460 nm in a Bio-Tek Synergy H4 microplate reader. Kinetic curves were generated with GraphPad Prism.

Cellular thermal stability assays: Experiment to determine ADT-007 binding to RAS in cells was performed by Cellaris Bio LLC (San Diego, CA) using HCT-116 and HT-29 cells cultured in RPMI medium supplemented with 10% FBS. For an initial determination of the melting profile of KRAS, fresh cell lysates were prepared in non-denaturing buffer was cleared via centrifugation at 5.000 rpm for 15 min. Cleared lysates were dispensed into 96-well PCR (equivalent of

approx. 6000 cells/well/50 µl), then subjected to temperature gradient (38-65°C) for 10 min. Subsequently, centrifugation was performed at 14.000 rpm to sediment the unstable protein content. Following WB of the soluble fraction, bands of stable KRAS were quantified, normalized to DMSO, and plotted using GraphPad Prism software. Non-linear regression analysis was used to fit a Sigmoidal dose-response curve with variable slope to generate EC_{50} values for ADT-007 binding to KRAS.

Additional cellular thermal stability experiments used a Micro-Tag enzyme complementation method. A KRAS G12C Micro-Tag construct was engineered having a 15-amino acid tag at the N-terminus. The construct was transiently expressed in HEK293 cells. Two days post-transfection cells were lifted, washed with Tris Buffered Saline (TBS: 20mM Tris HCl pH 7.4, 150mM NaCl) and re-suspended at 1000 cells/µl in TBS and 50,000 cells aliquoted to wells of a PCR plate. Increasing doses of ADT-007 and a control compound (ADT-652) were added and incubated with cells for 45min followed by heating for 10min at 55°C and a 1min cool down on ice. An equal volume of 0.5% Triton-X-100 in TBS was added, and cells lysed for 10min on ice followed by addition of the Tag binding protein and substrate and immediately proceeded to measurement of fluorescence signal. Fluorescence signal was plotted with concentration of the compounds on a semi-log scale using GraphPad Prism 9.0 software. Non-linear regression analysis was used to fit a Sigmoidal dose-response curve with variable slope to generate EC_{50} values for ADT-007 binding to KRAS.

<u>RAS Activation Assays</u>: Cells were grown to 80 percent confluence using complete growth medium then washed with 1 mL of PBS and lysed on ice for 5 min, (25 mM Tris HCl, 150 mM NaCl, 5 mM $MgCl_2$, 1% NP-40, 5% glycerol, pH 7.2) with Halt Protease and Phosphatase Inhibitor Cocktail (Thermo Fisher Scientific), then clarified at 16,000 RCF 15 minutes at 4°C. Protein concentration of the supernatant was normalized using the DC protein assay (Bio-Rad). 200 µg of whole cell lysate was incubated with GST-RAF-RBD (Addgene) bound to glutathione

agarose beads at 4°C for 1 hour. Bound active RAS was collected by centrifugation at 6,000 RCF for 30 seconds at 4°C, washed thrice with lysis buffer, then eluted with SDS sample buffer and subsequently detected by WB with a Pan-RAS antibody or isotype specific antibody as described below.

Western blotting: Tumor or cell lysates were generated after treatment with 500 uL RIPA lysis buffer (Thermo Scientific, 89900) with protease and phosphatase inhibitors (Thermo Scientific, 78440), boiled for 5 minutes and equal protein concentrations were loaded and run on a 12% SDS-PAGE. Gels were transferred to a PVDF membrane, which were blocked with either 5% non-fat dry milk in TBS-T (TBS with 0.1% Tween 20) or 5% BSA in TBS-T, depending on the blocking agent used for the primary antibodies, for 1 hour at room temperature. Membranes were incubated overnight at 4°C on a rocker with primary antibodies **(Supplemental Table 2**) according to the manufacturer's instructions and then developed with HRP-conjugated secondary antibodies (Cell Signaling Technology) for 1 hour at room temperature on an orbital shaker. Membranes were developed using SuperSignal West Enhanced Chemiluminescent substrate (Thermo Fisher Scientific) and imaged using a ChemiDoc Imaging System (Bio-Rad).

Tumor cell implantation and ADT-007 treatment: A single cell suspension of murine CRC or PDA cells was prepared in PBS and kept on ice until injection. $1x10^6$ syngeneic mouse CRC and PDA tumor cells were injected subcutaneously into 6–8-week-old BALB/C or C57BL/6 mice, respectively. When tumors reached an average tumor volume of 150 mm^3 mice began receiving daily intra-tumoral (10 mg/kg, QD, 7 days/week for 17-21 days) or peri-tumoral (5 mg/kg, BID, 7 days/week for 17-21 days). Tumor growth was assessed by caliper measurements (2-3/week) and tumor volumes ($TV = W \times L^2/2$) were calculated throughout the study. No overt signs of toxicity (body weight loss or organ [lungs, heart, liver, GI tract] pathology) were noted with local administration.

Flow Cytometry: Mouse tumors were digested in a 1 mg/mL collagenase IV and 0.1 mg/mL DNAase 1 (Worthington Biochemical, Lakewood, NJ) in HBSS for 45 minutes at 37 °C with intermittent shaking. Samples were then washed with RPMI containing 10% FBS and filtered through a 70μM strainer generating single cell suspensions. Cells were labeled with primary fluorophore-conjugated antibodies and a live/dead stain (**Supplemental Table 3**) for 30-60 min at 4 °C, washed and re-suspended in flow buffer. Cytokine expression from single cell suspensions of spleen and tumor was quantified as follows: cells were plated at a concentration of 10^6 cells in 1 mL of RP-10 media and stimulated for 5 hours at 37 °C using a 1x solution of a Cell Activation Cocktail containing PMA ionomycin, and Brefeldin A (Biolegend, San Diego, CA). Conversely, cells were cultured for 5 hours at 37°C using a solution containing 5 ug of Brefeldin A (BioLegend, San Diego, CA) to serve as an unstimulated control. After cell surface staining, cells were fixed in 4% paraformaldehyde for 45 minutes at 4 °C then washed with 1x Perm/Wash (BD, 554723). For intracellular staining in tumor and spleen samples, cells were stained with an antibody cocktail specific intracellular cytokines (IL-2, IFNγ, TNFα, and granzyme B) in Perm/Wash solution for 60 minutes at 4 °C. Data were acquired on a Symphony A5 flow cytometer, with analysis performed using FlowJo version 10.7.2.

Statistical Analyses: GraphPad Prism (version 9.1.2) was used for statistical analyses and graphical representation with data are presented as either means ± standard deviation (SD) or standard error of the mean (SEM). Two-tailed Student's t-test and Two-way Analysis of Variance (ANOVA) with multiple corrections (Bonnferoni method) were performed for determination of statistical significance between groups. For IC_{50} generation, concentrations were log transformed, data were then normalized to control and *log*(inhibitor) vs. response (four parameter nonlinear dose-response) test was used. A $p < 0.05$ was considered statistically significant.

Data Availability: The data generated in this study are available upon request from the corresponding author.

RESULTS

ADT-007 potently and selectively inhibits the growth of cancer cells with mutated or activated RAS

A library of indenes was synthesized and screened for differential growth inhibitory activity using HCT-116 CRC cells harboring a $KRAS^{G13D}$ mutation vs. HT-29 CRC cells with RAS^{WT} but mutant $BRAF^{V600E}$. A lead compound, ADT-007 (**Figure 1A**), and a series of analogs emerged following extensive chemical optimization for potency and selectivity. ADT-007 inhibited the growth of HCT-116 cells with an IC_{50} of 5 nM, while HT-29 cells were approximately 100-fold less sensitive with an IC_{50} of 493 nM (**Figure 1B**). As expected, HCT-116 cells expressed high levels of activated RAS (GTP-RAS) as measured by RAS-RBD pulldown assays that were undetectable in HT-29 cells (**Figure 1B**). Despite differences in activated RAS levels, both cell lines depended on MAPK signaling for growth, given comparable sensitivity to inhibitors targeting downstream kinases, RAF, MEK, and ERK in growth assays (data not shown). The requirement of mutant or activated RAS for sensitivity to ADT-007 was determined by transfecting HT-29 cells with $HRAS^{G12V}$. ADT-007 treatment of transfected cells resulted in an IC_{50} of 24 nM in growth assays compared with IC_{50} values of 549 and 730 nM for parental and vector control cells, respectively (**Figure 1C**).

We further evaluated the growth inhibitory activity of ADT-007 using a large panel of histologically diverse cancer cell lines with various mutations in RAS isozymes or upstream signaling components that activate or regulate RAS such as RTK or GTPase activating proteins (GAPS), respectively (**Table 1**). Cancer cell lines with mutations in K/N/HRAS isozymes or

upstream signaling components (e.g., PDGF, EGFR, or NF1) were uniformly sensitive to ADT-007 with growth IC_{50} values in the single-digit nM range. In contrast, cancer cell lines with RAS^{WT} but with downstream BRAF mutations were essentially insensitive to ADT-007. Normal colonocytes (NCM460) or airway epithelium cells (NHAEC) were also insensitive to ADT-007 treatment.

$KRAS^{G12C}$ MIA PaCa-2 PDA cells were highly sensitive to ADT-007 with IC_{50} values as low as 2 nM in growth assays, resulting in a selectivity index approaching 1200-fold relative to RAS^{WT} BxPC-3 PDA cells (**Table 1 and Supplemental Figure 1A**). RAS-RBD pulldown assays confirmed high levels of GTP-RAS in MIA PaCa-2 and three other PDA cell lines that were sensitive to ADT-007 and harbor $KRAS^{G12V}$ and $KRAS^{G12D}$ mutations (**Supplemental Figure 1B**), representing the most prevalent KRAS mutations in PDA patients [26]. By comparison, activated RAS levels in RAS^{WT} BxPC-3 cells were undetectable in RAS-RBD pulldown assays. As observed for HT-29 cells, transfecting BxPC-3 cells with mutant $KRAS^{G12C}$ induced sensitivity to ADT-007 in growth assays (**Supplemental Figure 1C**). The introduction of activated RAS BxPC-3 cells by transfection was confirmed by RBD pulldown assays (**Supplemental Figure 1D**).

Other experiments showed that ADT-007 treatment of MIA PaCa-2 cells comparably blocked growth in 2D monolayer and 3D spheroid cultures, resulting in unusually steep dose-response curves, which was a characteristic feature of ADT-007 and related analogs, indicating a highly uniform response of the cells to treatment (**Supplemental Figure 1E-F**). ADT-007 also completely inhibited the colony formation of KRAS mutant PDA cell lines without significantly affecting the colony formation of BxPC-3 cells (**Supplemental Figure 1G**).

ADT-007 inhibits activated RAS and MAPK/AKT signaling in human CRC and PDA cell lines

We next evaluated the effect of ADT-007 on RAS activation and RAS-dependent signaling in RAS mutant cancer cell lines. ADT-007 caused a concentration-dependent reduction of RAS-GTP levels and phosphorylated c-RAF, MEK, ERK, and AKT components of MAPK and PI3K signaling in HCT-116 cells (**Figure 1D**). Similar effects of ADT-007 treatment on levels of phosphorylated MAPK and PI3K signaling components were observed in MIA PaCa-2 cells that were serum-starved and treated with ADT-007, followed by EGF stimulation (**Figure 1E**). ADT-007 reduction of RAS-GTP levels occurred under multiple conditions when MIA PaCa-2 cells were grown in the presence of serum, serum-starved, or serum-starved and EGF stimulated (**Supplemental Figures 2A-C**). Pan-RAS inhibitory activity of ADT-007 was confirmed by experiments showing that ADT-007 treatment of MIA PaCa-2 cells reduced levels of GTP-HRAS^{WT} and GTP-NRAS^{WT} isozymes that were co-expressed with GTP-KRAS^{G12C} (**Figure 1F**). As expected, EGF did not increase GTP-KRAS^{G12C} levels but only activated GTP-HRAS^{WT} and GTP-NRAS^{WT} isozymes. Nonetheless, ADT-007 reduced mutant KRAS isozyme levels to the same extent as EGF-activated RAS^{WT} isozymes.

Comparison with mutant-specific KRAS inhibitors

We also compared the anticancer activity of ADT-007 with the KRAS^{G12C} inhibitor, AMG-510 (sotorasib), and the pan-KRAS inhibitor, BI-2865. AMG-510 and BI-2865 were significantly less potent and caused much less growth inhibition than ADT-007 in growth assays involving MIA PaCa-2 cells (Figure 1**G**). In addition, the growth of LLC cells harboring dual mutations, KRAS^{G12C} and NRAS^{Q61H}, was only partially inhibited by BI-2865, whereas ADT-007 retained activity (**Figure 1H**). LLC cells were insensitive to AMG-510 (**Figure 1I**), as previously reported [27], but retained sensitivity to ADT-007. These results show that ADT-007 has appreciably greater intrinsic anticancer activity and maintains potency in the presence of two independent activating RAS mutations compared with sotorasib, which is known from clinical trials to have modest efficacy and prone to resistance from the acquisition of additional cis- or trans-mutations in RAS alleles [21, 28].

ADT-007 blockade of RAS activation and MAPK/AKT signaling induced cell cycle arrest and apoptosis

We also examined the effect of ADT-007 treatment on cell cycle distribution and apoptosis. ADT-007 induced G2/M cell cycle arrest in HCT-116 and MIA PaCa-2 cells at concentrations within the range of growth IC_{50} values, while HT-29 and BxPC-3 cells displayed profoundly reduced sensitivity (**Supplemental Figure 3A-D**). ADT-007 also increased levels of active, cleaved caspase-3 protein in MIA PaCa-2 cells, which followed effects on cell cycle arrest (**Supplemental Figure 3E**). Similar findings were noted with HCT-116 cells and by measuring apoptosis using Annexin as a marker of apoptosis (data not shown). Given the effect of ADT-007 on G2/M arrest and previous studies suggesting that certain other indenes non-selectively bind tubulin [29], the impact of ADT-007 on tubulin polymerization was determined using recombinant α-tubulin. ADT-007 exhibited a weak inhibitory effect on tubulin polymerization at a concentration 100-fold above its growth IC_{50} value, making a direct link between effects on tubulin polymerization and cell cycle arrest unlikely (**Supplemental Figure 3F**). Similar weak effects on tubulin polymerization were observed by treating RAS mutant cancer cells with ADT-007 at growth IC_{50} values.

Metabolic mechanisms impacting resistance and sensitivity to ADT-007

As described above, ADT-007 reduced activated RAS at concentrations effective for inhibiting growth. The potency and selectivity of ADT-007 to inhibit RAS-dependent growth and reduce activated RAS was significantly diminished when the hydroxyl moiety on the phenolic ring was substituted with a methoxy moiety as shown with a trimethoxy analog, ADT-106 (**Figure 2A-B**). The results show exquisite chemical selectivity for inhibiting RAS-dependent growth and biological selectivity linked with reducing activated RAS.

As discussed below*, ex vivo* treatment of mouse liver microsomes with ADT-007 followed by LC-MS/MS analysis of metabolites revealed that the hydroxyl moiety is rapidly

glucuronidated by UDP-glucuronosyltransferases (UGTs) (**Supplemental Figure 5A-B**). These results suggested that high UGT levels known to be expressed in normal cells could account for insensitivity to ADT-007. Measurement of UGT protein levels by WB using a pan-UGT1 antibody revealed lower UGT expression in sensitive RAS mutant HCT-116 and MIA PaCa-2 cells lines compared with insensitive RAS^{WT} HT-29 and BxPC-3 cell lines (**Figure 2C-D**). Evaluation of transcriptomic data (RNAseq) of most of the cell lines in **Table 1** (Cancer Cell Line Encyclopedia) [30] describing mRNA expression of six distinct UDP-glucuronosyltransferase isoforms (UGT1A1, 1A6, 1A10, 2A1, 2B10, and 2B15) provided additional evidence for lower UGT expression RAS mutant sensitive vs. RAS^{WT} sensitive cell lines to ADT-007 (**Table 1, Supplemental Table 1**). Measurement of ADT-007 levels by LC-MS/MS from cells treated overnight with ADT-007 revealed 350-fold higher intracellular levels in sensitive RAS mutant HCT-116 cells than insensitive RAS^{WT} HT-29 cells. Consistent with the ability of UGTs to deactivate ADT-007, a higher ratio of the glucuronide-conjugated form of ADT-007 was measured in HT-29 cells, while none was detected in HCT-116 cells (**Figure 2E-F**). Experiments using a competitive UGT inhibitor, propofol, supported these observations by showing that pretreatment increased the sensitivity of RAS^{WT} HT-29 and BxPC3 cells to ADT-007 in growth assays, decreasing the IC_{50} value by 26- and 18-fold, respectively, without significantly affecting the sensitivity of RAS mutant HCT-116 or MIA PaCa-2 cells to ADT-007 (**Supplemental Table 4**).

ADT-007 binds RAS

The ability of ADT-007 to directly bind KRAS in cells was measured using two different cellular thermal stability assays based on the principle that a protein maintains thermal stability when in a conformation favorably for binding to a small molecule inhibitor. Initial experiments measured the optimal temperature to denature 75% (T_{agg75}) KRAS in whole cell lysates, followed by WB quantification of non-denatured KRAS levels. Treating HCT-116 lysates with

ADT-007 increased KRAS^{G13D} thermal stability (T_{agg75}), resulting in an EC_{50} of 0.45 nM for ADT-007 to bind KRAS. By comparison, ADT-007 did not affect the thermal stability of KRAS^{WT} in HT-29 cells **(Figure 3A)**. As a control, ADT-007 did impact the thermal stability of an unrelated protein (PDE10) in either HCT-116 or HT-29 cells (data not shown), previously reported to be comparably expressed in both cell lines [31]. Additional experiments were conducted involving ADT-007 treatment of intact HEK293 embryonic kidney cells transfected with epitope-tagged mutant KRAS^{G12C} and detection of thermal stability by WB analysis with anti-Micro-Tag antibody. These experiments resulted in an EC_{50} value of 8.5 nM for ADT-007 to bind KRAS (**Figure 3B**). A trimethoxy analog of ADT-007 (ADT-652) lacking RAS selectivity in growth assays used as a control compound did not significantly bind KRAS in transfected KRAS^{G12C} HEK293 embryonic kidney cells. These results indicate direct binding of ADT-007 to mutant RAS in cells with an affinity consistent with potency to inhibit growth.

Molecular docking studies using KRAS^{WT} (PDB ID 4OBE) [32] were conducted to understand how ADT-007 may bind RAS. The studies used molecular dynamics and induced fit docking to identify potential binding sites for ADT-007 on KRAS. Simulations were performed with either Mg^{+2} present or Mg^{+2} removed since it was uncertain which conformation of RAS would be the more favorable for ADT-007 binding **(Supplemental Figure 4A-B)**. A difference was observed in the orientation of ADT-007 within its predicted binding sites when Mg^{+2} was present versus when absent **(Supplemental Figure 4C-D)**. When Mg^{+2} was present, the phenolic OH group of ADT-007 was predicted to H-bond with S17 through a water bridge and with E31 through a direct H-bond. When Mg^{+2} was absent, the phenolic OH was predicted to interact with D119 via a water bridge and A146 by a direct H-bond. In simulations of Mg^{+2} being present and absent, the best GLIDE docking scores (-11.08 and -12.06, respectively) were calculated with ADT-007 binding to a site partially overlapping the nucleotide binding site that was associated with an altered conformation of the switch-1 region **(Supplemental Figure 4A-**

B). Regardless if Mg^{+2} was present or absent, the GLIDE docking score of GDP to bind RAS (-9.6 and -8.80, respectively) was considerably less favorable than ADT-007. These results suggested that a conformational change induced by the binding of ADT-007 may decrease the affinity for nucleotide. The results also indicate there may be a preference for ADT-007 binding to RAS in a conformation when Mg^{+2} is absent as nucleotide-free RAS (nf-RAS) and that ADT-007 bound better to this site than nucleotide.

ADT-007 binds nucleotide-free RAS and inhibits GTP activation

Next, we determined whether ADT-007 could inhibit GTP loading to nf-RAS and GDP-bound RAS using a recombinant full-length $KRAS^{WT}$ protein. To confirm the binding of ADT-007 to nf-RAS, recombinant full-length $KRAS^{WT}$ was treated with EDTA to chelate the Mg^{+2}, thereby simulating GEF removal of GDP, producing the apoenzyme bearing the nucleotide-free conformation of RAS. ADT-007 treatment of RAS before GTP addition inhibited RAS activation as determined by measuring GTP-RAS levels with RAS-RBD pulldown assays. This effect occurred at concentrations comparable to growth IC_{50} values and to a similar extent as GDP-RAS controls (**Figure 3C**). However, there was a negligible effect of ADT-007 on activated RAS levels when RAS was preloaded with GTP (**Figure 3D**). These results are consistent with molecular modeling observations suggesting that nf-RAS is the preferred conformation for ADT-007 to bind RAS. In addition to RAS-RBD pulldown assays, we utilized a nucleotide exchange assay to determine the effect of ADT-007 on the kinetics of GTP binding to $KRAS^{WT}$ using a fluorescent GTP analog (Mant-GTP). These experiments showed that ADT-007 reduced the rate of GTP binding to RAS if pretreated with EDTA to chelate Mg^{2+} (**Figure 3E**) but not after adding non-hydrolyzable GTPγS (**Figure 3F**). A tool compound, CID1067700, previously reported as a pan GTPase inhibitor, also inhibited Mant-GTP binding to RAS to a comparable extent as ADT-007 (data not shown) [33].

We also used protein nuclear magnetic resonance (NMR) spectroscopy to define the molecular determinants for these biochemical findings. First, we compared ^{15}N-HSQC spectra of GDP-KRAS^{WT} protein alone and GDP-KRAS^{WT} in the presence of ADT-007. The lack of spectral differences under these conditions suggests a low likelihood of direct binding of ADT-007 to inactive GDP-KRAS (data not shown). To further investigate the binding of ADT-007 to RAS, Mg^{2+} was chelated with EDTA to generate nf-RAS. These conditions allow the dissociation of GDP from KRAS, producing a sample with NMR spectral features distinct from GDP-KRAS. Treatment of nf-RAS with ADT-007 led to attenuation of several HN signals, including signals for G13, a hotspot mutation site in the P-loop [34], and at K16 (adjacent to S17) (**Figure 4**), which is critical for Mg^{2+} binding [35]. These discrete signals can readily be assigned due to their unique resonance frequencies. NMR signal attenuation in the presence of ADT-007 indicates direct binding of ADT-007 to KRAS, leading to an intermediate exchange between the compound-occupied and free KRAS or altered backbone dynamics in the compound binding site.

ADT-007 inhibits mouse colon tumor growth and RAS signaling *in vivo*

As mentioned above, *ex vivo* treatment of mouse liver microsome with ADT-007 followed by LC-MS/MS analysis of metabolites identified a metabolic vulnerability of ADT-007 to be rapidly metabolized by glucuronidation (**Supplemental Figure 5A-B**). ADT-007 was, however, stable in mouse plasma (**Supplemental Figure 5C**), which prompted studies to evaluate antitumor activity from localized delivery to minimize hepatic glucuronidation. Antitumor activity of ADT-007 was initially evaluated at a dose of 5 mg/kg for 14 days (BID) by peri-tumoral injection. In the KRAS^{G12V} gall bladder adenocarcinoma (GBA) PDX model, ADT-007 completely arrested tumor growth and induced partial regression (**Figure 5A, left and right panels**). ADT-007 also caused growth arrest in a KRAS^{G12C} PDA PDX model by peritumoral injection (data not shown). Localized treatment by intraperitoneal injection of ADT-007 was also determined using

three peritoneal metastasis PDX models bearing mutant $KRAS^{G12A}$ (PMCA-1) (**Figure 5B**), $KRAS^{G12D}$ (PMP1) (**Figure 5C**), or $KRAS^{WT}$ and $PDGFR^{T922I}$ (PC244) (**Figure 5D**). Representative growth curves (**Figure 5B-D, left panels**) and tumor volumes at the end of treatment (right panels) are displayed for each model system (**Figure 5B-D, right panels**). ADT-007 significantly reduced tumor growth in all three models. Of the three models, PMCA-1 was the most sensitive, where the growth inhibitory activity persisted for a substantial time after treatment discontinuation, and two mice were deemed as cured or tumor-free on day 100. Consistent with experiments described above involving cancer cell lines (**Table 1**), the PC244 PDX model expressing RAS^{WT} isozymes, but a suspected activating mutation in PDGFR, was comparably sensitive to ADT-007 *in vivo*. Furthermore, reductions in mucin production were notable by MRI (**Supplemental Figure 6A**) with tumor volumes exhibiting a dose dependency in each model (**Supplemental Figure 6B-D**). These findings indicate that ADT-007 induces tumor growth arrest and, in some cases, tumor regression of established and metastatic PDX PDA and CRC tumors in immune-deficient recipient mouse models.

The antitumor activity of ADT-007 was also determined against an array of syngeneic, CRC and PDA tumor models bearing $KRAS^{G12D}$ mutations using immune-competent mice. When administered locally by intratumor (IT) injection, ADT-007 (10 mg/kg, qd) strongly inhibited SC tumor growth (T/C_{max} of 27%) in the KRAS mutant CT26 colon tumor model (**Figure 5E, left panel**) with an 80% reduction in mean tumor growth compared to sham-treated mice (**Figure 5E, right panel**), which correlated with reduced levels of activated RAS and phosphorylated MAPK components (RAF, MEK, and ERK) compared with control mice (**Supplemental Figure 7**). Peritumoral administration of ADT-007 (5 mg/kg, BID, administered for 17-24 days) induced growth arrest in syngeneic mouse PDA models including previously characterized cell lines 2838c3 (**Figure 5F, left panel**) and 7160c2 (**Figure 5G, left panel**) [36], and a novel KPC cell line 5363 (**Figure 5H, left panel**) with variable patterns of growth arrest to

regression noted (**Figure 5F-H, right panels**). These findings indicate that ADT-007 inhibits *in vivo* growth of mouse and human tumor models bearing different KRAS mutations or those exhibiting hyperactivation of WT KRAS.

We next developed a prodrug approach to achieve systemic levels of ADT-007 by oral administration. A carbamate prodrug of ADT-007 coded as ADT-316 was synthesized to protect the vulnerable hydroxyl group from glucuronidation (**Supplemental Figure 5D**). Oral administration of ADT-316 provided plasma levels of ADT-007 approximately 10-fold higher than growth inhibitory IC_{50} values (**Supplemental Figure 5E**) and displayed antitumor activity in a SC CT26 murine CRC model at a dosage that was well tolerated (**Supplemental Figure 5F**). However, PK analysis of plasma levels of ADT-316 and ADT-007 revealed incomplete conversion of the prodrug to ADT-007 (**Supplemental Figure 5E**), which likely accounts for its modest antitumor activity and supports the need for further development of prodrugs or analogs as discussed below.

ADT-007-mediated inhibition of $KRAS^{G12D}$ alters the tumor immune microenvironment (TiME)

Given the impact of mutant-specific $KRAS^{G12C}$ [19, 37] and $KRAS^{G12D}$ inhibitors [38] on tumor-specific immunity, as previously reported, we assessed the activity of ADT-007 in syngeneic, immune-competent mouse models of CRC and PDA-bearing $KRAS^{G12D}$ mutation. To evaluate the effect of ADT-007 on the PDA TiME, we studied two genetically characterized cell lines bearing increased T cell infiltrate (2838c3 and 7160c2) but exhibiting different abundances of myeloid cells, basal levels of T cell activation, and function [36]. At the termination of treatment, 2838c3 and 7160c2 tumor-bearing mice were euthanized, and tumors were collected to evaluate changes in YFP^+ tumor and $CD11b^+$ $CD11c^+$ myeloid cell subsets within the TiME. In both models, ADT-007 decreased the proportion of YFP^+ tumor cells (**Figure 6A and I**).

Using multiparameter flow cytometry (**Supplemental Figure 8A**), proportions of myeloid subsets with the 7160c2 and 2838c3 PDA TiME were evaluated. A direct comparison between myeloid abundances in each model (sham-treated) revealed that 2838c3 had an increase in overall proportions and abundance of myeloid cells compared to 7160c2 with significant increases in Ly6G^{+} Ly6C^{+} granulocytes (**Supplemental Figure 8B**). After treatment, an increase in proportions of CD11b^{+} Ly6G^{+} Ly6C^{+} gMDSC and CD11b^{+} Ly6G^{-} Ly6C^{hi} mMDSC subsets was noted in 7160c2, but in ADT-007 treated 2838c3 tumor-bearing mice, which exhibited a decrease in macrophages (**Figure 6B***,7160c2* and **5J***,2838c3*). No changes in dendritic cell subset (cDC1, cDC2, CD103^{+} DC) numbers were noted in either model (**Figures 6C***,7160c2* and **5I-K***,2838c3*). Analysis of CD11b^{+} F4/80^{+} macrophage phenotypes in both models revealed trends for decreasing MHCII and CD206 expression (**Supplemental Figure 8C***,7160c2* and **Supplemental Figure 8D**,2838c3).

Next we evaluated the importance of T and B cells in ADT-007 efficacy in 2838c3 and 7160c2 PDA models using both immune-competent C57BL/6 mice or immune-deficient C57BL/6 Rag 1$^{-/-}$ mice. Treatment with ADT-007 reduced growth in both immune-competent C57BL/6 and immune-deficient C57BL/6 Rag 1$^{-/-}$ mice, however, efficacy was reduced in C57BL/6 Rag 1$^{-/-}$ recipient mice with both models (**Figure 6D***,7160c2* and **6L***,2838c3*). The effect of ADT-007 on T and NK cell numbers, activation, and cytokine production in 7160c2 and 2838c3 TiME was evaluated using multiparameter flow cytometry (**Supplemental Figure 9A**). An initial comparison between sham treatment groups for 2838c3 and 7160c2 revealed a modest but statistically insignificant increase in overall CD3^{+} T cell numbers in the 2838c3 model (**Supplemental Figure 9B**). However, after ADT-007 treatment numbers of γδ, NKT, and NK cells increased within the TiME in both models (**Figure 6E-F***, 7160c2* **and 6M-N***, 2838c3*). Additionally, in the 2838c3 TiME, an increase in CD3^{+} CD4/8^{-} TCRγδ^{-} DN T cells was noted (**Figure 6M**). The activation/memory status of T cell subsets was evaluated by CD44 and

CD62L expression (**Supplemental Figure 9A**). T cell phenotypes in the 7160c2 TiME shifted to a CD44^{hi} CD62L^{-}effector memory phenotype with ADT-007 treatment (**Supplemental Figure 9C)**. In comparison, ADT-007 treatment of 2838c3 tumors increased proportions of pre-effector and effector memory phenotypes in the CD4^{+} Foxp3^{-} and CD3^{+} TCRγδ^{+} T cell subsets (**Supplemental Figure 9D** and data not shown). Expression of PD-1 increased on CD4 and CD8^{+} T cells in 7610c2 (**Supplemental Figure 10A**, 7160c2 and **B***, 2838c3*), but not 2838c3 TiME, despite higher baseline levels of PD-1 on T cells (**Supplemental Figure 10C**). Evaluation of PD-1 and TIM-3 co-expression as an indicator of an exhausted T cell state revealed a modest trend for co-expression in T cells in 7160c2 but not 2838c3 TiME (**Supplemental Figure 10D-E**). Analysis of T cell infiltrates in the CT-26 TiME revealed trends for increased numbers, PD-1 expression (not statistically significant), and reduced CTLA-4 expression in both CD4^{+} and CD8^{+} T cell subsets (data not shown).

Functional assessments of IL-2, IFNγ, TNFα, and granzyme B production in T cell subsets from 7160c2 and 2838c3 TiME was performed by intracellular staining after PMA and ionomycin stimulation. In the 7160c2 TiME both CD4^{+} and CD8^{+} T cells exhibited increased expression of IL-2, granzyme B, IFNγ, and TNFα (**Figure 6G-H**), whereas minimal changes in cytokine expression were noted in T cells within the 2838c3 TiME (**Figure 6O-P**). Functional differences as evidenced by the production of IL-2, IFNγ, TNFα, and granzyme B, were not apparent in CD4^{+} and CD8^{+} T cells within the CT-26 TiME (data not shown). Using an IFNγ-Thy1.1 reporter model system [39] we assessed vivo IFNγ production marked by surface Thy1.1 on innate and adaptive T and NK subsets as an indicator of cytotoxic activity. Consistent with ICS resulst, ADT-007 increased IFNγ production in T cell subsets in the 7160c2, but not 2838c3 PDA TiME. In NK, NKT, and γδ T cells, IFNγ was unchanged (**Supplemental Figure 11A***, 7160c2* **and 11B***, 2838c3*) whereas, a significant decrease in Thy1.1 was noted in NK cells from ADT-007 treated tumors (**Supplemental Figure 11A***, 7160c2* **and 11B***, 2838c3*). Overall, these

findings show that ADT-007 modulates the innate and adaptive immunity in CRC and PDA TiME and suggests a role for the adaptive immune system in enhancing ADT-007 efficacy.

Discussion

ADT-007 potently and selectively inhibited the growth of cancer cell lines with mutant RAS or activated RAS^{WT} from mutations in upstream signaling molecules by binding RAS to block GTP-activation of MAPK/AKT signaling, resulting in cell cycle arrest and apoptosis. Despite its broad anticancer activity, ADT-007 displayed exquisite selectivity as cancer cell lines with RAS^{WT} and downstream mutation in BRAF, as well as cells from normal tissues, were essentially insensitive in growth assays. ADT-007 displayed high affinity to bind RAS in cells with EC_{50} values in the same range as concentrations required to inhibit growth, colony formation, and induce cell cycle arrest and apoptosis, which were also in the same range as concentrations effective for reducing RAS-GTP levels and blocking MAPK/AKT signaling. The inhibitory effect of ADT-007 on RAS-GTP levels was apparent under standard growth conditions, serum-free conditions, or following EGF stimulation. As a pan-RAS inhibitor, ADT-007 reduced RAS-GTP levels of mutant KRAS and co-expressed WT HRAS and NRAS isozymes, which we suspect will be advantageous over mutant-specific or pan-KRAS inhibitors.

Localized delivery of ADT-007 strongly inhibited tumor growth in immunodeficient and syngeneic murine models of CRC and PDA with partial dependence on the adaptive immune system. ADT-007 activated T cells and enhanced their cytotoxic functions in $KRAS^{G12D}$ mutated CRC and PDA, immune-competent mouse models. Oral delivery of a prototypic prodrug, ADT-316, generated adequate plasma levels to inhibit tumor growth but with modest efficacy, which we attribute to incomplete hydrolysis of the prodrug moiety to ADT-007. Recognizing the limitations of ADT-316, we designed a new series of prodrugs that are currently under study, one of which shows robust antitumor activity in mouse, human cell line, and patient-derived

models of PDA and is in further development by the National Cancer Institute Stepping Stones Program.

ADT-007 specificity for RAS binding

ADT-007 appears to preferentially bind nf-RAS to block GTP activation of effector interactions, which, to our knowledge, is the first-ever reported small molecule to inhibit RAS by this mechanism. Molecular modeling studies revealed that ADT-007 generated the highest docking score when RAS is in a nucleotide-free conformation. Biochemical experiments using recombinant RAS showed that ADT-007 inhibited GTP binding to RAS and GTP-dependent RAS-RAF binding under nucleotide-free conditions. NMR spectroscopy confirmed these observations by showing binding to nf-RAS but not nucleotide-loaded RAS. Previous studies reporting that a fraction of RAS exists in cells in a nucleotide-free state [40] support the ability of ADT-007 to inhibit RAS-dependent growth by binding nf-RAS within the nucleotide-binding domain to block GTP activation of effector interactions.

Cellular thermal stability assays provided additional evidence for direct binding of ADT-007 to RAS in cells, showing that exposure of lysates from $KRAS^{G13D}$ mutant HCT-116 cells to ADT-007 resulted in sub-nanomolar EC_{50} values to bind RAS but not in RAS^{WT} HT-29 cells. In addition, ADT-007 treatment of intact $KRAS^{WT}$ HEK293 cells transfected with a $KRAS^{G12C}$ mutant allele resulted in EC_{50} values for binding RAS comparable to growth IC_{50} values. The lack of binding of ADT-007 in HT-29 cells may be attributed to low levels of activated RAS or, as discussed below, also attributed to metabolic deactivation by UGT isozymes remaining active in cell lysates. Nonetheless, results from experiments involving transfection of mutant RAS into RAS^{WT} cancer cells led us to conclude that activated RAS from either a mutation or upstream signaling is necessary and sufficient for the sensitivity of cancer cells to ADT-007.

Metabolic deactivation of ADT-007 by UGT-mediated glucuronidation is also a significant factor impacting sensitivity to treatment that has implications for the interpretation of *in vitro* and *in vivo* experiments. Liver microsome experiments revealed that ADT-007 is rapidly

glucuronidated by UGT enzymes, ubiquitously expressed in normal tissues, and known to metabolize compounds with phenolic OH moieties. Unexpectedly, cancer cells with WT RAS had high mRNA and protein levels of major UGT isozymes expressed in normal cells. In contrast, cancer cells with mutant RAS had low levels of UGT isozymes. Measurement of cellular levels of ADT-007 following overnight treatment with ADT-007 using LC-MS/MS confirmed high ADT-007 levels and undetectable ADT-007 glucuronide levels in HCT-116 cells, but low ADT-007 levels and high ADT-007 glucuronide levels in HT-29 cells. In addition, pretreatment with a known competitive UGT inhibitor, propofol, increased sensitivity in resistant HT-29 and BxPC-3 cancer cell lines with low activated RAS to ADT-007. Propofol pretreatment did not significantly impact cells with mutant KRAS and low UGT levels. These results suggest that UGT-mediated glucuronidation allows bystander cells from normal tissues to be protected from pan-RAS inhibition by ADT-007 and contributes to its unique selectivity despite previous reports that knock-out of all three RAS isozymes is lethal to mice [41, 42]. While UGT isozymes are expressed in metabolic tissues such as the liver, colon, and kidney, they are also expressed in other normal tissues, including blood cells, and regulated by multiple signaling pathways and transcription factors [43]. These results support further study of the relationship between RAS mutational status and UGT isozyme expression.

Other indenes chemically related to ADT-007 were previously reported to inhibit cancer cell growth by a dual mechanism involving inhibition of cyclic guanine monophosphate phosphodiesterase (cGMP PDE) activity and tubulin polymerization [29]. The former was based on reports that certain sulindac derivatives inhibit cGMP PDE activity at concentrations that inhibit CRC cell growth [23, 44]. The latter was hypothesized due to the chemical resemblance of certain indenes containing a trimethoxy substitution with colchicine, which is well known to bind tubulin and disrupt microtubule assembly [45]. We, therefore, determined if ADT-007 inhibited cGMP PDE activity by measuring effects on cGMP hydrolysis using recombinant PDE10, a cGMP-degrading PDE isozyme, or capacity to bind PDE10 in cells using cellular

thermal stability assays. However, we found no evidence of PDE10 inhibition or binding at concentrations within a range that effectively inhibited growth. In addition, ADT-007 only inhibited tubulin polymerization at concentrations ~100-fold higher than growth IC_{50} values. These observations indicate that neither cGMP PDE nor tubulin polymerization inhibition likely accounts for the anticancer activity of ADT-007. Moreover, reports that tubulin inhibitors induce MAPK pathway activity [46], rather than inhibit MAPK signaling provide further evidence that ADT-007 does not target tubulin. However, the likelihood that ADT-007 inhibits RAS and, at higher concentrations, also inhibits tubulin polymerization suggests additional therapeutic advantages, given that both RAS and tubulin are well-validated anticancer targets.

ADT-007 inhibits a wide range of RAS-addicted tumors and circumvents resistance involving reactivation of the RAS pathway

Unlike mutant-specific KRAS or pan-KRAS inhibitors [47], ADT-007 exhibited broad anticancer activity for mutant K/H/NRAS isozymes inhibiting downstream MAPK/AKT signaling, resulting in cell cycle arrest and apoptosis. The broad anticancer activity of ADT-007 supports its potential to be developed as a generalizable monotherapy for patients with PDA, given that 94% of patients diagnosed with this malignancy have multiple KRAS mutations [26] and a significant proportion of patients with WT KRAS have RTK fusions that would be predicted to have hyper-activated RAS^{WT} isozymes [48]. Furthermore, evidence indicates that ADT-007 exhibits high potency in tumor cells with activated RAS signaling, which may provide greater therapeutic utility in patients with metastatic disease in which the proliferation of cancer cells depends upon activated KRAS signaling for survival in the metastatic niche [49]. ADT-007 exhibits potent growth inhibition *in vitro* and *in vivo* with syngeneic $KRAS^{G12D}$ mutated CRC and PDA cell lines and human $KRAS^{G12C}$ and $KRAS^{G12V}$ mutated PDA and CC PDX models consistent with its pan-RAS inhibitory activity.

Equally important to the broad activity of this class of compounds is the potential to provide a second-line therapy for patients with RAS mutant cancers that develop resistance to

mutant-specific KRAS inhibitors. In NSCLC patients who go on to develop resistance to $KRAS^{G12C}$ mutant-specific inhibitors, the majority of resistance pathways involve further modulation of RAS signaling, including polyclonal mutations in RAS or upstream receptor tyrosine kinases or GTPase that result in dysregulated RAS^{WT} signaling [7, 22]. Our findings indicate that ADT-007 fully maintains activity in MIA PaCa-2 cell lines that develop resistance to sotorasib and adagrasib (not shown) and in LLC cells with $KRAS^{G12C}$ $NRAS^{Q61H}$ dual mutations [27].

ADT-007 modulates the tumor immune microenvironment

ADT-007-mediated *in vivo* tumor growth inhibition appears to be partially dependent upon the adaptive immune response as evidenced by reduced growth inhibitory activity of ADT-007 on 2838c3 tumor cell growth in immune-deficient Rag $1^{-/-}$ mice lacking B and T cells. Similar findings have been observed with $KRAS^{G12C}$ [19, 37] and $KRAS^{G12D}$-specific inhibitors [38], which demonstrated that T cells either contributed to the efficacy of targeted mutation-specific KRAS inhibitors or are critical for their long-term control of regrowth from microscopic disease [38] in different syngeneic mouse PDA models. Furthermore, the presence of T cells predicted the response to PD-1 immune checkpoint blockade in preclinical models of NSCLC and PDA. [37, 50].

In T cell inflamed PDA tumor models (2838c3 and 7160c2), ADT-007 treatment increased numbers of innate-like T lymphocytes (NK T, γδT, and DN T) and NK cells, whereas conventional $CD4^+$ and $CD8^+$ T cell numbers did not change. In the CRC model, CT-26, trends for increases in conventional $CD4^+$ and $CD8^+$ T cells were consistently measured, although variable in statistical significance. In the 7160c2 TiME, ADT-007 treatment increased proportions of $CD44^{hi}$ $CD62L^-$ effector memory T cells and production of T_H1 cytokines, including IL-2, TNFα, IFNγ, and the cytotoxic protein granzyme B. Although increased production of these cytokines was not observed in the $CD4^+$ and $CD8^+$ T cells in the 2838c3 model, increased proportions of effector T cells and higher levels of PD-1 expression were

observed when compared to $CD4^+$ and $CD8^+$ T cells within the 7160c2 TiME consistent with previous findings [36]. Analysis of *in vivo* production of IFNγ using Thy1.1-IFNγ reporter mice revealed that most adaptive and innate-like T cells were $Thy1.1^+$, consistent with IFNγ production. These findings suggest role(s) for innate and adaptive immune response in contributing to the antitumor activity of ADT-007.

In conclusion, we believe this novel class of pan-RAS inhibitors has strong potential to address the complex genetic landscape of RAS-driven cancers. The results support further development of ADT-007 analogs and prodrugs with oral bioavailability as a generalizable monotherapy or combined with other RAS pathway-directed inhibitors or immunotherapy.

References

1. Siegel RL, Giaquinto AN, Jemal A. Cancer statistics, 2024. *CA Cancer J Clin* **2024**;74(1):12-49.
2. Yang Y, Zhang H, Huang S, Chu Q. KRAS Mutations in Solid Tumors: Characteristics, Current Therapeutic Strategy, and Potential Treatment Exploration. *J Clin Med* **2023**;12(2):709.
3. Hingorani SR, Petricoin EF, Maitra A, Rajapakse V, King C, Jacobetz MA, *et al*: Preinvasive and invasive ductal pancreatic cancer and its early detection in the mouse. *Cancer Cell* **2003**; 4(6):437-450.
4. Kojima K, Vickers SM, Adsay NV, Jhala NC, Kim HG, Schoeb TR, et al. Inactivation of Smad4 accelerates Kras(G12D)-mediated pancreatic neoplasia. *Cancer Res* **2007**;67(17):8121-8130.
5. Boutin AT, Liao WT, Wang M, Hwang SS, Karpinets TV, Cheung H, *et al*: Oncogenic Kras drives invasion and maintains metastases in colorectal cancer. *Genes Dev* **2017**;31(4):370-382.
6. Bardeesy N, Aguirre AJ, Chu GC, Cheng KH, Lopez LV, Hezel AF, *et al*. Both p16(Ink4a) and the p19(Arf)-p53 pathway constrain progression of pancreatic adenocarcinoma in the mouse. *Proc Natl Acad Sci U S A* **2006**;103(15):5947-5952.
7. Sheffels E, Kortum RL. The Role of Wild-Type RAS in Oncogenic RAS Transformation. *Genes (Basel)* **2021**;12(5):662.
8. Ying H, Kimmelman AC, Lyssiotis CA, Hua S, Chu GC, Fletcher-Sananikone E, *et al*: Oncogenic Kras maintains pancreatic tumors through regulation of anabolic glucose metabolism. *Cell* **2012**; 149(3):656-670.
9. Mukhopadhyay S, Goswami D, Adiseshaiah PP, Burgan W, Yi M, Guerin TM, et al. Undermining Glutaminolysis Bolsters Chemotherapy While NRF2 Promotes Chemoresistance in KRAS-Driven Pancreatic Cancers. *Cancer Res* **2020**;80(8):1630-1643.
10. Collins MA, Brisset JC, Zhang Y, Bednar F, Pierre J, Heist KA, et al. Metastatic pancreatic cancer is dependent on oncogenic Kras in mice. *PLoS One* **2012**;7(12):e49707.
11. Zhang Y, Yan W, Collins MA, Bednar F, Rakshit S, Zetter BR, et al. Interleukin-6 is required for pancreatic cancer progression by promoting MAPK signaling activation and oxidative stress resistance. *Cancer Res* **2013**;73(20):6359-6374.
12. Zdanov S, Mandapathil M, Abu Eid R, Adamson-Fadeyi S, Wilson W, Qian J, *et al*. Mutant KRAS Conversion of Conventional T Cells into Regulatory T Cells. *Cancer Immunol Res* **2016**;4(4):354-365.
13. Bayne LJ, Beatty GL, Jhala N, Clark CE, Rhim AD, Stanger BZ, et al. Tumor-derived granulocyte-macrophage colony-stimulating factor regulates myeloid inflammation and T cell immunity in pancreatic cancer. *Cancer Cell* **2012**;21(6):822-835.
14. Ischenko I, D'Amico S, Rao M, Li J, Hayman MJ, Powers S, et al. KRAS drives immune evasion in a genetic model of pancreatic cancer. *Nat Commun* **2021**;12(1):1482.
15. Coelho MA, de Carne Trecesson S, Rana S, Zecchin D, Moore C, Molina-Arcas M, *et al*. Oncogenic RAS Signaling Promotes Tumor Immunoresistance by Stabilizing PD-L1 mRNA. *Immunity* **2017**; 47(6):1083-1099 e1086.
16. Muthalagu N, Monteverde T, Raffo-Iraolagoitia X, Wiesheu R, Whyte D, Hedley A, *et al*. Repression of the Type I Interferon Pathway Underlies MYC- and KRAS-Dependent Evasion of NK and B Cells in Pancreatic Ductal Adenocarcinoma. *Cancer Discov* **2020**;10(6):872-887.

17. Stalnecker CA, Der CJ. RAS, wanted dead or alive: Advances in targeting RAS mutant cancers. *Sci Signal* **2020**;13(624).
18. Kwan AK, Piazza GA, Keeton AB, Leite CA. The path to the clinic: a comprehensive review on direct KRAS(G12C) inhibitors. *J Exp Clin Cancer Res* **2022**;41(1):27.
19. Canon J, Rex K, Saiki AY, Mohr C, Cooke K, Bagal D, *et al*: The clinical KRAS(G12C) inhibitor AMG 510 drives anti-tumour immunity. *Nature* **2019**;575(7781):217-223.
20. Li BT, Falchook GS, Durm GA, Burns TF, Skoulidis F, Ramalingam SS, *et al*. CodeBreaK 100/101: First Report of Safety/Efficacy of Sotorasib in Combination with Pembrolizumab or Atezolizumab in Advanced KRAS p.G12C NSCLC. *J Thorac Oncol* **2022**;17(9S):S10.
21. Ryan MB, Fece de la Cruz F, Phat S, Myers DT, Wong E, Shahzade HA, *et al.* Vertical Pathway Inhibition Overcomes Adaptive Feedback Resistance to KRAS(G12C) Inhibition. *Clinical cancer research : an official journal of the American Association for Cancer Research* **2020**;26(7):1633-1643.
22. Awad MM, Liu S, Rybkin, II, Arbour KC, Dilly J, Zhu VW, *et al*: Acquired Resistance to KRAS(G12C) Inhibition in Cancer. *N Engl J Med* **2021**;384(25):2382-2393.
23. Thompson HJ, Jiang C, Lu J, Mehta RG, Piazza GA, Paranka NS, *et al.* Sulfone metabolite of sulindac inhibits mammary carcinogenesis. *Cancer Res* **1997**;57(2):267-271.
24. Herrmann C, Block C, Geisen C, Haas K, Weber C, Winde G, *et al.* Sulindac sulfide inhibits Ras signaling. *Oncogene* **1998**;17(14):1769-1776.
25. Karaguni IM, Glüsenkamp KH, Langerak A, Geisen C, Ullrich V, Winde G, *et al.* New indene-derivatives with anti-proliferative properties. *Bioorg Med Chem Lett* 2002, 12(4):709-713.
26. Waters AM, Der CJ. KRAS: The Critical Driver and Therapeutic Target for Pancreatic Cancer. *Cold Spring Harb Perspect Med* **2018**;8(9):a031435.
27. Molina-Arcas M, Moore C, Rana S, van Maldegem F, Mugarza E, Romero-Clavijo P, *et al*. Development of combination therapies to maximize the impact of KRAS-G12C inhibitors in lung cancer. *Sci Transl Med* **2019**;11(510):eaaw7999.
28. Tanaka N, Lin JJ, Li C, Ryan MB, Zhang J, Kiedrowski LA, *et al.* Clinical Acquired Resistance to KRAS(G12C) Inhibition through a Novel KRAS Switch-II Pocket Mutation and Polyclonal Alterations Converging on RAS-MAPK Reactivation. *Cancer Discov* **2021**;11(8):1913-1922.
29. Xiao D, Deguchi A, Gundersen GG, Oehlen B, Arnold L, Weinstein IB. The sulindac derivatives OSI-461, OSIP486823, and OSIP487703 arrest colon cancer cells in mitosis by causing microtubule depolymerization. *Mol Cancer Ther* **2006**;5(1):60-67.
30. Barretina J, Caponigro G, Stransky N, Venkatesan K, Margolin AA, Kim S, *et al*. The Cancer Cell Line Encyclopedia enables predictive modelling of anticancer drug sensitivity. *Nature* **2012**; 483(7391):603-607.
31. Lee KJ, Chang WL, Chen X, Valiyaveettil J, Ramirez-Alcantara V, Gavin E, *et al*. Suppression of Colon Tumorigenesis in Mutant Apc Mice by a Novel PDE10 Inhibitor that Reduces Oncogenic β-Catenin. *Cancer Prev Res (Phila)* **2021**;14(11):995-1008.
32. Hunter JC, Gurbani D, Ficarro SB, Carrasco MA, Lim SM, Choi HG, *et al*. In situ selectivity profiling and crystal structure of SML-8-73-1, an active site inhibitor of oncogenic K-Ras G12C. *Proc Natl Acad Sci U S A* **2014**;111(24):8895-8900.
33. Agola JO, Hong L, Surviladze Z, Ursu O, Waller A, Strouse JJ, *et al*. A competitive nucleotide binding inhibitor: in vitro characterization of Rab7 GTPase inhibition. *ACS chemical biology* **2012**; 7(6):1095-1108.
34. Hunter JC, Manandhar A, Carrasco MA, Gurbani D, Gondi S, Westover KD. Biochemical and Structural Analysis of Common Cancer-Associated KRAS Mutations. *Molecular cancer research : MCR* **2015**;13(9):1325-1335.

35. John J, Rensland H, Schlichting I, Vetter I, Borasio GD, Goody RS, *et al.* Kinetic and structural analysis of the Mg(2+)-binding site of the guanine nucleotide-binding protein p21H-ras. *The Journal of biological chemistry* **1993**;268(2):923-929.
36. Li J, Byrne KT, Yan F, Yamazoe T, Chen Z, Baslan T, *et al*. Tumor Cell-Intrinsic Factors Underlie Heterogeneity of Immune Cell Infiltration and Response to Immunotherapy. *Immunity* **2018**; 49(1):178-193 e177.
37. Mugarza E, van Maldegem F, Boumelha J, Moore C, Rana S, Llorian Sopena M, *et al*. Therapeutic KRAS(G12C) inhibition drives effective interferon-mediated antitumor immunity in immunogenic lung cancers. *Sci Adv* **2022**;8(29):eabm8780.
38. Kemp SB, Cheng N, Markosyan N, Sor R, Kim IK, Hallin J, *et al*. Efficacy of a Small-Molecule Inhibitor of KrasG12D in Immunocompetent Models of Pancreatic Cancer. *Cancer Discov* **2023**; 13(2):298-311.
39. Harrington LE, Janowski KM, Oliver JR, Zajac AJ, Weaver CT. Memory CD4 T cells emerge from effector T-cell progenitors. *Nature* **2008**;452(7185):356-360.
40. Khan I, Koide A, Zuberi M, Ketavarapu G, Denbaum E, Teng KW, *et al*. Identification of the nucleotide-free state as a therapeutic vulnerability for inhibition of selected oncogenic RAS mutants. *Cell Rep* **2022**;38(6):110322.
41. Esteban LM, Vicario-Abejon C, Fernandez-Salguero P, Fernandez-Medarde A, Swaminathan N, Yienger K, *et al*. Targeted genomic disruption of H-ras and N-ras, individually or in combination, reveals the dispensability of both loci for mouse growth and development. *Mol Cell Biol* **2001**; 21(5):1444-1452.
42. Johnson L, Greenbaum D, Cichowski K, Mercer K, Murphy E, Schmitt E, *et al*: K-ras is an essential gene in the mouse with partial functional overlap with N-ras. *Genes Dev* **1997**;11(19):2468-2481.
43. Allain EP, Rouleau M, Lévesque E, Guillemette C. Emerging roles for UDP-glucuronosyltransferases in drug resistance and cancer progression. *Br J Cancer* **2020**; 122(9):1277-1287.
44. Tinsley HN, Gary BD, Thaiparambil J, Li N, Lu W, Li Y,*et al.* Colon tumor cell growth-inhibitory activity of sulindac sulfide and other nonsteroidal anti-inflammatory drugs is associated with phosphodiesterase 5 inhibition. *Cancer Prev Res (Phila)* **2010**;3(10):1303-1313.
45. Lu Y, Chen J, Xiao M, Li W, Miller DD. An overview of tubulin inhibitors that interact with the colchicine binding site. *Pharm Res* **2012**;29(11):2943-2971.
46. Waters AM, Khatib TO, Papke B, Goodwin CM, Hobbs GA, Diehl JN, *et al*: Targeting p130Cas- and microtubule-dependent MYC regulation sensitizes pancreatic cancer to ERK MAPK inhibition. *Cell Rep* **2021**;35(13):109291.
47. Coley AB, Ward A, Keeton AB, Chen X, Maxuitenko Y, Prakash A, *et al.* Pan-RAS inhibitors: Hitting multiple RAS isozymes with one stone. *Adv Cancer Res* **2022**;153:131-168.
48. Luchini C, Paolino G, Mattiolo P, Piredda ML, Cavaliere A, Gaule M, *et al*. KRAS wild-type pancreatic ductal adenocarcinoma: molecular pathology and therapeutic opportunities. *J Exp Clin Cancer Res* **2020**;39(1):227.
49. di Magliano MP, Logsdon CD. Roles for KRAS in pancreatic tumor development and progression. *Gastroenterology* **2013**;144(6):1220-1229.
50. Mahadevan KK, McAndrews KM, LeBleu VS, Yang S, Lyu H, Li B, *et al*. KRAS(G12D) inhibition reprograms the microenvironment of early and advanced pancreatic cancer to promote FAS-mediated killing by CD8(+) T cells. *Cancer Cell* **2023**;41(9):1606-1620 e1608.
51. Flatmark K, Reed W, Halvorsen T, Sorensen O, Wiig JN, Larsen SG, *et al.* Pseudomyxoma peritonei--two novel orthotopic mouse models portray the PMCA-I histopathologic subtype. *BMC Cancer* **2007**;7:116.

52. Flatmark K, Davidson B, Kristian A, Stavnes HT, Førsund M, Reed W. Exploring the peritoneal surface malignancy phenotype—a pilot immunohistochemical study of human pseudomyxoma peritonei and derived animal models. *Human Pathology* **2010**;41(8):1109-1119.
53. Fleten KG, Lund-Andersen C, Waagene S, Abrahamsen TW, Mørch Y, Boye K, *et al.* Experimental Treatment of Mucinous Peritoneal Metastases Using Patient-Derived Xenograft Models. *Translational oncology* **2020**;13(8):100793.

Figures and Figure Legends:

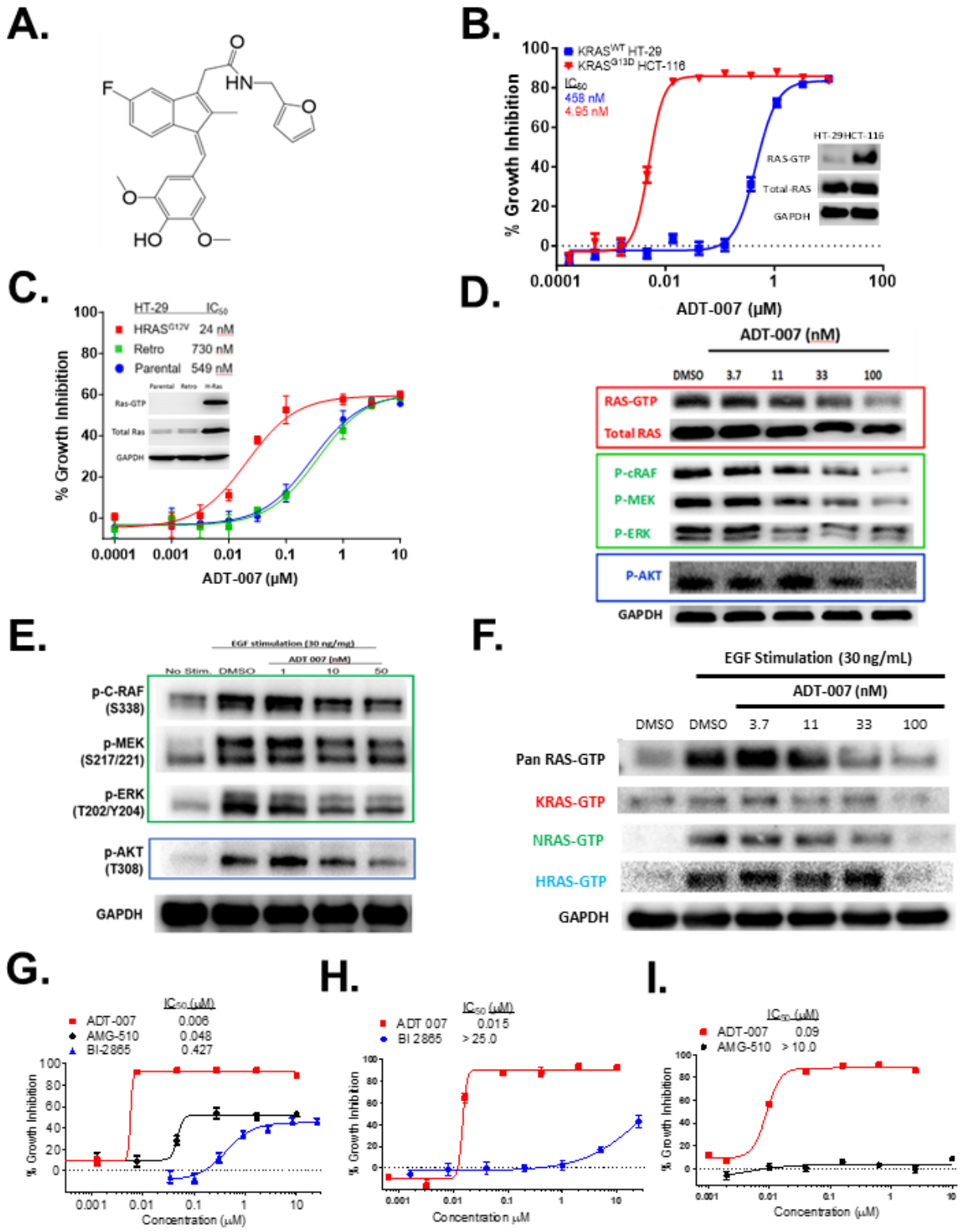

Figure 1. ADT-007 inhibits activation of mutant and RAS^{WT} isozymes and downstream

MAPK signaling circumventing resistance. (A) Chemical structure of ADT-007. **(B)** ADT-007 inhibition of $KRAS^{G13D}$ HCT-116 vs. $KRAS^{WT}$, $BRAF^{V600E}$ HT-29 growth following 72 hours of treatment (CellTiter-Glo ATP content Assay; (CTG))**.** Quadruplicate samples ± standard error of the mean (SEM). Inset: Activated RAS-GTP-RBD pulldown evaluated by pan-RAS western (WB). Total RAS and GAPDH were evaluated by WB. **(C)** Ectopic expression of $HRAS^{G12V}$ sensitized HT-29 cells to ADT-007 growth inhibition (quadruplicates ± SEM). Inset: Activated RAS in untreated parental, vector control (retro), and transfected ($HRAS^{G12V}$). (**D**) HCT-116 $KRAS^{G13D}$ cells were treated with increasing concentrations of ADT-007 overnight in complete medium (10% FBS). Activated RAS-GTP pulldowns, phospho(P)-cRAF, P-MEK, P-ERK, total RAS and GAPDH as loading controls were detected by WB. Data represent 3 independent experiments. (**E,F**) Serum-starved MIA PaCa-2 $KRAS^{G12C}$ PDA cells were treated overnight with vehicle or increasing concentrations of ADT-007, then EGF stimulated (10 min). (**E)** P-cRAF, P-MEK, P-ERK, P-AKT and GAPDH as loading controls were detected by WB. Data represent 2 independent experiments. (**F**) Activated RAS-GTP was isolated by RAS-RBD pulldown followed by WB with pan-RAS, KRAS, HRAS, or NRAS specific antibodies and GAPDH control. Data represent at least two independent experiments. Growth inhibition of LLC cells (**G, H**; $KRAS^{G12C}$ / $NRAS^{Q61H}$) or MIA PaCa-2 cells (**I**; $KRAS^{G12C}$) by ADT-007 vs BI-2865 or AMG-510.

Type	Tissue Origin	Cell Line	Mutation Status	IC_{50} (nM)	UGT1A10
Mutant RAS, sensitive	Pancreatic	MIA PaCa-2	KRAS G12C	2.1	0.263
	Pancreatic	PANC-1	KRAS G12D	2.4	0.043
	Pancreatic	SW-1990	KRAS G12D	6.3	0.138
	Lung	A549	KRAS G12S	6.8	0.070
	Pancreatic	CFPAC-1	KRAS G12V	5.8	2.63
	Colon	SW480	KRAS G12V	6.5	0.58
	Breast	MDA-MB-231	KRAS G13D	3.6	0.043
	Colon	HCT-116	KRAS G13D	4.7	0
	Ovarian	OVCAR-8	KRAS P121H	5.8	0.057
	Breast	Hs 578T	HRAS G12D	3.9	0.098
	Skin	SK-MEL-2	NRAS Q61K	2.1	0
	Lung	NCI-H1299	NRAS Q61K	2.4	0
WT RAS, resistant	Normal Lung	NHAEC	WT RAS	19100	*
	Normal Colon	NCM460	WT RAS	50000	*
Downstream mutation (WT RAS) resistant	Ovarian	OV-90	WT RAS/mut BRAF	350	4.57
	Colon	HT-29	WT RAS/mut BRAF	512	6.97
	Skin	SK-MEL-28	WT RAS/mut BRAF	> 25,000	0.14 (3.53†)
	Pancreatic	BxPC-3	WT RAS/mut BRAF	2500	7.75
Upstream RAS activation sensitive	Lung	NCI-H1975	WT RAS/mut EGFR	3.9	*
	Skin (mouse)	B16	WT RAS/mut PDGFR	5.8	*
	Brain	U-87 MG	WT RAS/mut NF1	1.6	0
	Ovarian	SK-OV-3	WT RAS/mut NF1	6.7	0.202

Table 1. ADT-007 sensitivity is associated with high activated RAS and low UGT superfamily enzyme levels. Growth inhibitory (IC_{50}) values following 72 hours of treatment (CTG assay). TPM normalized expression of the most significant differentially expressed UGT1A10 enzyme from published data (Cancer Cell Line Encyclopedia; DepMap Portal; Broad Institute). * expression data not available, † TPM normalized UGT2B7 expression in SK-MEL-28.

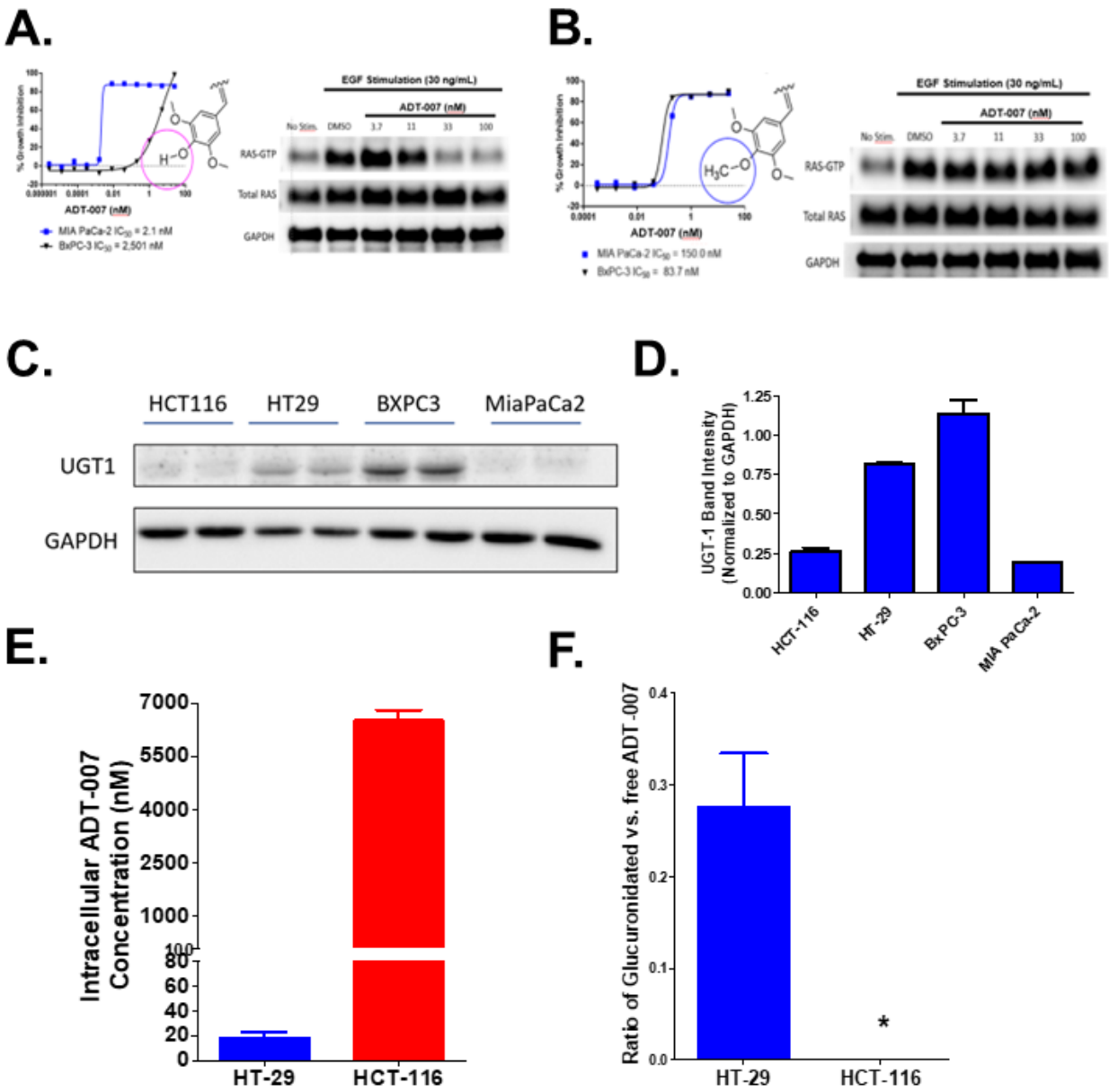

Figure 2. Phenolic moiety is critical for RAS selectivity of ADT-007-. (A) Left panel: ADT-007 selectively inhibits growth of mutant KRAS^{G12C} MIA PaCa-2 PDA cells vs. KRAS^{WT} BxPC-3 (72h, CTG Assay; triplicates ± SEM). **(B)** Left panel: ADT-106 lacking a phenolic OH moiety was less potent (72h, CTG Assay; triplicates ± SEM). Right panels (**A, B**): Cells were treated for 18 hours, followed by activated RAS RAS-RBD pulldowns and WB analysis. **(C)** UGT1 protein expression in ADT-007 sensitive versus resistant cells by WB. (**D**) UGT1 protein expression and

control GAPDH (WB) were quantified and normalized (**E**) in image J. Representative of two independent experiments. **(E, F)** Mean ADT-007 and ADT-007-glucuronide were quantified in triplicate cell pellets by LC-MS/MS ± SEM), * = $p < 0.05$.

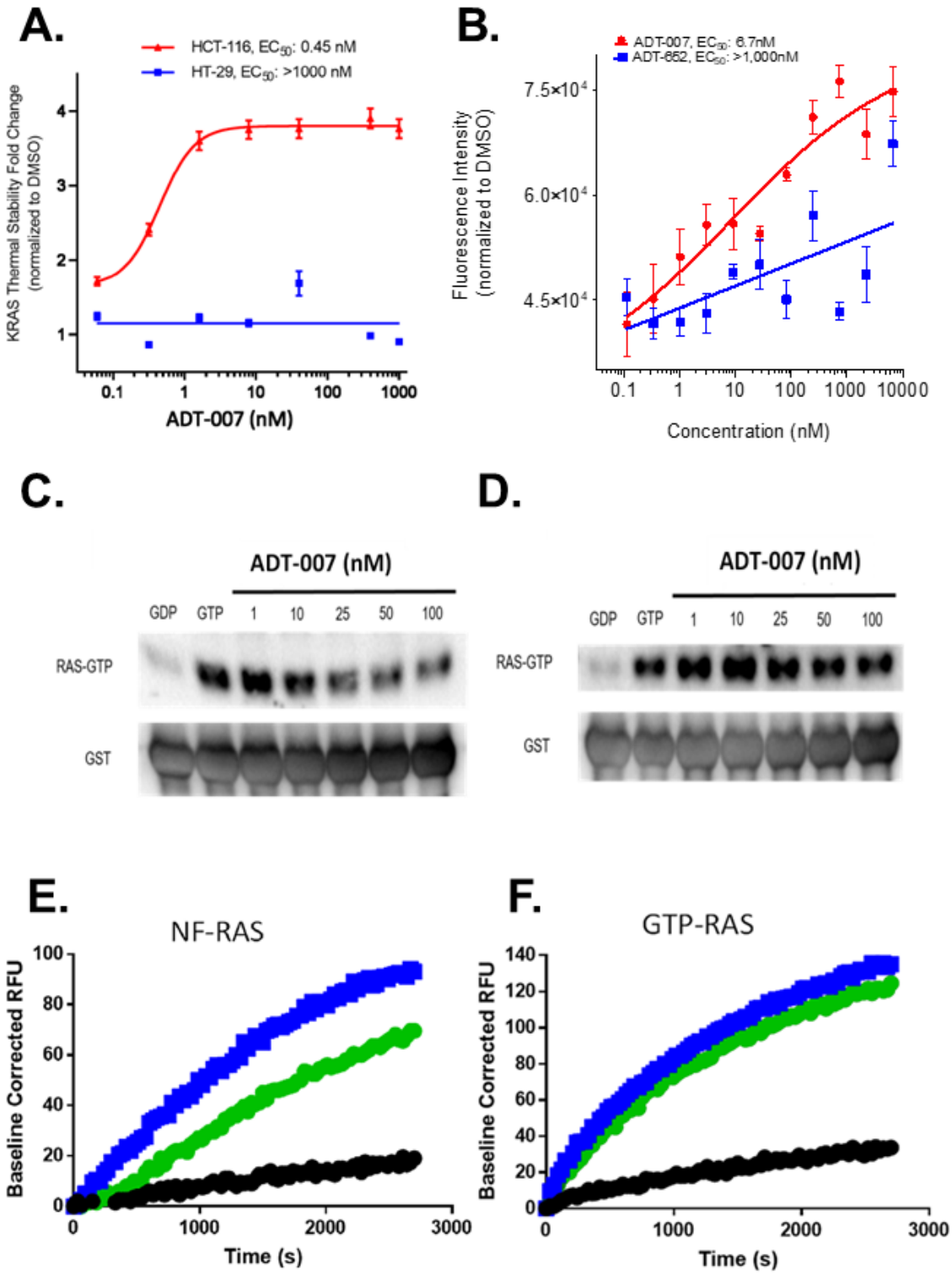

Figure 3. ADT-007 binds KRAS, inhibits nucleotide loading and effector binding. Cellular target engagement assays show: **(A)** ADT-007 binds KRAS with high affinity in $KRAS^{G13D}$ HCT-116 but not $KRAS^{WT}$ HT-29 CRC cells. Graphs show levels of compound stabilized KRAS

detected by WB compared with vehicle control. (**B**) Binding affinity of ADT-007 for mutant $KRAS^{G12C}$ was assessed by 45 min treatment of HEK293 cells expressing $KRAS^{G12C}$-Micro-Tag construct compared with a nonselective negative control compound. Curves are graphed as the average of two replicates ± SEM. **(C-D)** The inhibitory activity of ADT-007 to block recombinant $KRAS^{WT}$ activation (effector binding) in a cell-free system was evaluated by RAS-RBD pulldown assays. (**C**) ADT-007 inhibited $KRAS^{WT}$-RAF activation before GTP addition. **(D)** ADT-007 did not significantly inhibit $KRAS^{WT}$ activation / pulldown when added after GTP loading. (**E-F**) Kinetics of GTP binding to KRAS were measured using a fluorescent GTP analog (Mant-GTP). ADT-007 reduced the rate of Mant-GTP binding to KRAS if pretreated with EDTA to chelate Mg2+ (**E**), but not if added after non-hydrolysable GTPγS prior to incubation with ADT-007 (**F**). Data are representative of at least two independent experiments.

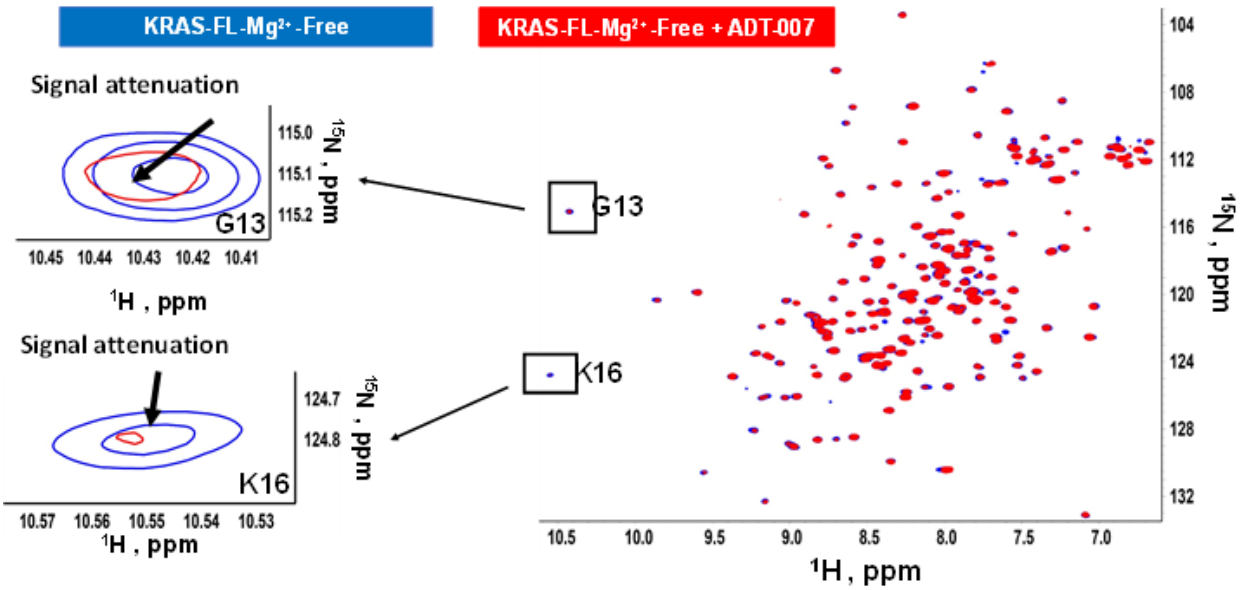

Figure 4. NMR analysis of ADT-007 binding to KRAS. Addition of ADT-007 (red) to Mg^{2+}-free KRAS (blue) (5:1 ratio) resulted in statistically significant NMR signal attenuation at G13 and K16 and other residues (described in methods). Assignments for G13 and K16 due to their unique resonance frequencies are shown as a larger image to the left.

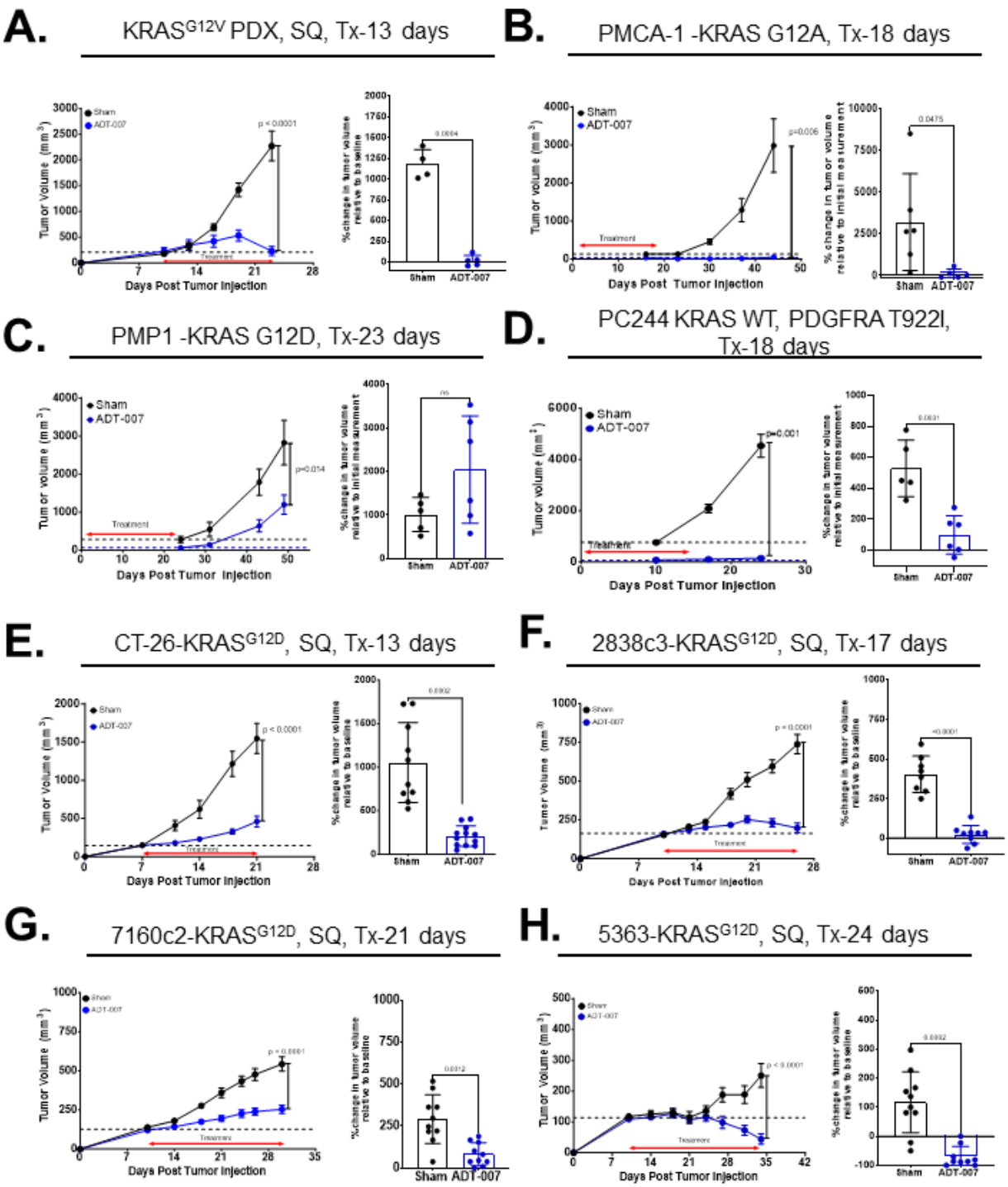

Figure 5. ADT-007 induces growth arrest and regression of CRC, GBA, and PDA cells *in vivo*. (**A**) Left panel: Growth inhibition of subcutaneous patient derived xenograft (PDX) gall bladder adenocarcinoma (GBA) bearing KRAS^{G12V} by peritumoral administration (5 mg/kg, BID,

13 days, n = 5 mice/group, mean ± SEM). Right panel: Percent change in tumor volume at endpoint compared to volume at start of treatment. (**B**-**D**) Left panels: Growth inhibition of peritoneal metastasis in mucinous colorectal adenocarcinoma models (**B**) PMCA1, (**C**) PMP1, and (**D**) PC244 in nude mice by IP administration of ADT-007 (2.5 mg/kg, BID) for treatment periods of 18 (PMCA1), 23 (PMP1), and 18 days (PC244). Treatment was initiated 24 hours after implantation (n = 5-6 mice/group, mean ± SEM) and mice were followed by MRI for a period of 24 to 50 days (6 – 31 days post treatment cessation) after implantation. Right panels: tumor sizes at end of treatment. (**E**) Left panel: Growth inhibition of subcutaneous CT26 colon tumors in BALB/c mice by IT administration of ADT-007 (10 mg/kg, QD, 13 days, mean ± SE, n=12). Right panel: Percent change in tumor volume at endpoint compared to volume at start of treatment. (**F-H**) Left panels: Growth inhibition studies of subcutaneous (**F**) 2838c3, (**G**) 7160c2, (**H**) 5363 PDA tumors in C57BL/6 mice by peritumoral administration of ADT-007 (5 mg/kg, BID) for treatment periods of 17 (2838c3), 21 (7160c2), and 24 (5363) days (n = 7 - 10 mice/group, mean ± SEM). Right Panels: Percent change in tumor volume at endpoint compared to volume at start of treatment. All animal studies are representative of 2-3 independent experiments. Left panels: Error bars are representative of SEM. Right panels: error bars are representative of SD. Left panels: Statistical significance was assessed using 2-way ANOVA with Sadik's multiple comparisons test. Right panels: Statistical significance was assessed with Welch's t-test. ** $p<0.001$, **** $p<0.0001$,

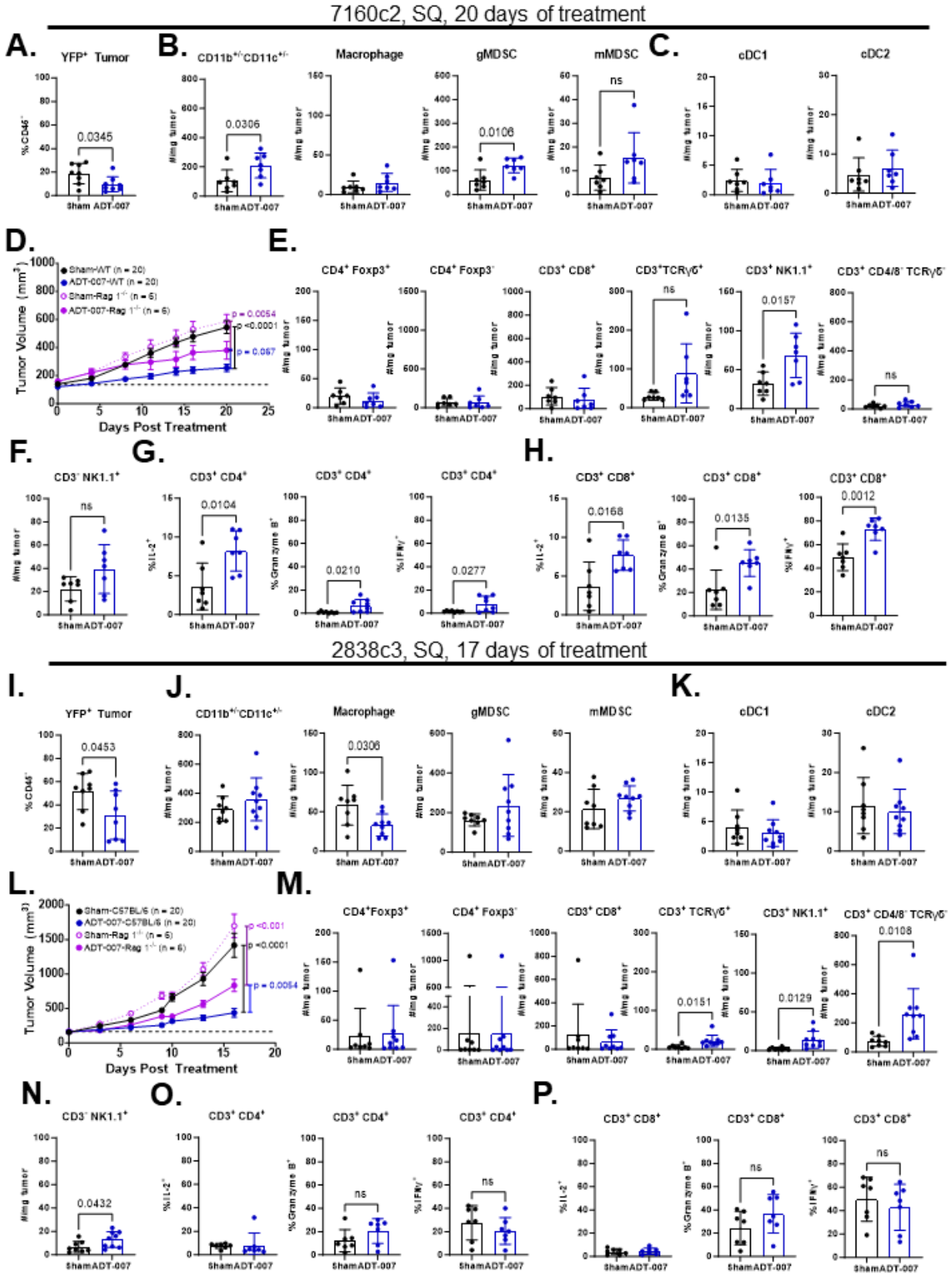
7160c2, SQ, 20 days of treatment
A.
YFP+ Tumor
0.0345
B.
CD11b+/-CD11c+/-
0.0306
Macrophage
gMDSC
0.0106
mMDSC
ns
C.
cDC1
cDC2
D.
Tumor Volume (mm3)
Days Post Treatment
Sham-WT (n = 20)
ADT-007-WT (n = 20)
Sham-Rag 1-/- (n = 6)
ADT-007-Rag 1-/- (n = 6)
p = 0.0054
p <0.0001
p = 0.067
E.
CD4+ Foxp3+
CD4+ Foxp3-
CD3+ CD8+
CD3+TCRγδ+
0.0157
CD3+ NK1.1+
CD3+ CD4/8- TCRγδ-
F.
CD3- NK1.1+
G.
CD3+ CD4+
0.0104
0.0210
0.0277
H.
CD3+ CD8+
0.0168
0.0135
0.0012
2838c3, SQ, 17 days of treatment
I.
YFP+ Tumor
0.0453
J.
CD11b+/-CD11c+/-
Macrophage
0.0306
gMDSC
mMDSC
K.
cDC1
cDC2
L.
Tumor Volume (mm3)
Days Post Treatment
Sham-C57BL/6 (n = 20)
ADT-007-C57BL/6 (n = 20)
Sham-Rag 1-/- (n = 6)
ADT-007-Rag 1-/- (n = 6)
p <0.001
p <0.0001
p = 0.0054
M.
CD4+Foxp3+
CD4+ Foxp3-
CD3+ CD8+
CD3+ TCRγδ+
0.0151
CD3+ NK1.1+
0.0129
CD3+ CD4/8- TCRγδ-
0.0108
N.
CD3- NK1.1+
0.0432
O.
CD3+ CD4+
ns
P.
CD3+ CD8+
ns
ShamADT-007

997

Figure 6. ADT-007 modulates myeloid subsets, induces T cell activation, and enhances cytotoxic function in PDA mouse models. (**A-H**) Data is from the 7160c2 PDA model. At 21 days of post treatment the proportions of tumor and myeloid cells were evaluated by multiparameter flow cytometry. (**A**) The percentages of $CD45^-$ YFP^+ tumor cells were decreased in ADT-007 treated mice (n = 8) compared to sham (n = 8). (**B**) The numbers/mg tumor of $CD11b^{+/-}$ $CD11c^{+/-}$ myeloid, $CD11b^+$ $Ly6G^+$ $Ly6C^+$ (gMDSC), and $CD11b^+$ $Ly6G^-$ $Ly6C^{hi}$ (mMDSC) in ADT-007 treated (n = 8) compared to sham (n = 8) treated mice. (**C**) The numbers/mg tumor of $CD11b^-$ $CD11c^{hi}$ $MHCII^{hi}$ $XCR1^+$ cDC1 and $CD11b^+$ $CD11c^{hi}$ $MHCII^{hi}$ $CD172\alpha^+$ cDC2 subsets in ADT-007 (n = 8) compared to sham (n = 8) treated mice. (**D**) Tumor growth in 7160c2 PDA tumor bearing C57BL/6 WT vs. C57BL/6 Rag $1^{-/-}$ mice by peritumoral administration (5 mg/kg, BID, days 7-28, n = 6-22 mice/group, mean $\pm$ SE). Data is an aggregate of 2 separate experiments. (**E**) The numbers/mg of tumor of $CD4^+$ $Foxp3^-$, $CD4^+$ $Foxp3^+$, $CD8^+$ T cells, $CD3^+$ $\gamma\delta TCR^+$($\gamma\delta$T), $CD3^+$ $NK1.1^+$(NKT) and $CD3^+$ $CD4/8^-$ $\gamma\delta TCR^-$ (DN) T cells and (**F**) $CD3^-$ $NK1.1^+$ NK cells in ADT-007 (n = 8) and sham (n = 8) treatment. (**G-H**) Intracellular cytokine (IL-2, granzyme B, and IFNγ) production (ICS) from (**G**) $CD4^+$ and (**H**) $CD8^+$ T cells isolated from the 7160c2 TME were evaluated after 5-hour stimulation with PMA/ionomycin in the presence of brefeldin A in ADT-007 (n = 8) or sham (n = 8) treated mice. (**I-P**) Data is from the 2838c3 PDA model. At 17 days post treatment the proportions of tumor and myeloid cells were evaluated by multiparameter flow cytometry. (**I**) The percentages of $CD45^-$ YFP^+ tumor cells were decreased in ADT-007 treated mice (n = 8) compared to sham (n = 8). (**J**) The numbers/mg tumor of myeloid, gMDSC, and mMDSC in ADT-007 treated (n = 8) and sham (n = 8) treated mice. (**K**) The numbers/mg tumor of cDC1 and cDC2 cells were evaluated in ADT-007 (n = 8) and sham (n = 8) treated mice. (**L**) Tumor growth in 2838c3 PDA tumor bearing C57BL/6 WT vs. C57BL/6 Rag $1^{-/-}$ mice by peritumoral administration (5 mg/kg, BID, days 7-24, n = 6-22 mice/group, mean $\pm$ SE). Data is an aggregate of 2 separate experiments. (**M**) Numbers/mg tumor of $CD4^+$ $Foxp3^-$, $CD4^+$ $Foxp3^+$, $CD8^+$, γδ, and DN T and

(**N**) NK cells in ADT-007 (n = 8) and sham (n = 8) treatment. (**O-P**) ICS assay results as described above on (**O**) $CD4^+$ and (**P**) $CD8^+$ T cells isolated from the 2838c3 TiME in ADT-007 (n = 8) or sham (n = 8) treated mice. For all column graphs, data is representative of 2 independent experiments. Statistic significance was calculated by Welch's t-test, ns indicates not significant. Error bars indicate SD. For evaluation of statistical significance in tumor growth curves 2way ANOVA with Tukey's multiple comparison test was used to calculate statistical significance. Error bars indicate SEM.

****$p < 0.0001$